

Structural and Functional Analysis of a Periplasmic Heme-binding Protein Involved in Bacterial Heme-acquisition Systems

Md. Mahfuzur Rahman

Doctoral Dissertation
2018

Department of Picobiology, Graduate School of Life Science
University of Hyogo, Hyogo, Japan

PUBLICATIONS LIST

1. Journal: Proteins: Structure, Function, and Bioinformatics, **85** (2017) 2217–2230

Title: Structural basis for binding and transfer of heme in bacterial heme-acquisition systems

Authors: Youichi Naoe*, Nozomi Nakamura*, Md. Mahfuzur Rahman*, Takehiko Tosha, Satoru Nagatoishi, Kouhei Tsumoto, Yoshitsugu Shiro, Hiroshi Sugimoto

* These three authors contributed equally to this work

Related paper

Journal: Biophysical Journal, **114**, Special issue 3 (2018) p424a*

Title: Crystal structure of a bacterial ABC heme exporter in the apo form

Authors: Md. Mahfuzur Rahman, Tamao Hisano, Hiro Nakamura, Yoshitsugu Shiro

*This is the supplemental issue as proceedings of the Biophysical Society Meeting 2018. As the original paper on this project is yet not published, it was not included in the thesis description.

Structural and functional analysis of a periplasmic heme-binding protein (PBP) involved in bacterial heme-acquisition systems

TABLE OF CONTENTS

1. ABSTRACT	1
2. INTRODUCTION	2
3. MATERIALS AND METHODS	6
3-1 Plasmid construction and protein expression	6
3-2 Protein purification	6
3-3 Spectroscopic titration experiments	7
3-4 Isothermal titration calorimetry (ITC) experiments	7
3-5 Crystallization	8
3-6 Optical absorption spectra	8
3-7 X-ray diffraction measurements, phase determination, and structure refinement	9
3-8 Resonance Raman spectroscopy	9
4. RESULTS	11
4-1 Protein purification and crystallization	11
4-2 Crystal structure of apo form	13
4-3 Heme-binding in solution	16
4-4 Thermodynamic analysis	18
4-5 Crystal structure of heme-bound form	20
4-6 Comparison of apo and heme-bound forms	23
4-7 Heme environmental structure in solution	25
4-8 Mutagenesis studies	27

5. DISCUSSION	37
5-1 Heme-binding mechanism of RhuT	37
5-2 Similarity and diversity of heme recognition in PBPs	38
5-3 Evolution of bacteria and PBPs	41
5-4 Conformational changes in PBPs during heme transfer to the transporter	42
6. CONCLUSION	46
7. REFERENCES	47
8. ACKNOWLEDGEMENTS	50

1. ABSTRACT

Periplasmic heme-binding proteins (PBPs) in Gram-negative bacteria are components of the heme-acquisition systems. These proteins shuttle heme across the periplasmic space from outer membrane receptors to ATP-binding cassette (ABC) heme importers located in the inner membrane. In the present study, X-ray crystallographic, spectroscopic and biochemical approaches were used to characterize a PBP (RhuT) from a thermophile *Roseiflexus* sp. RS-1. In solution, RhuT has the ability to bind two heme molecules sequentially depending on the heme concentration. The crystal structures of RhuT were solved in apo and 2-heme-bound forms at the resolution of 2.4 and 2.0 Å, respectively. The overall structure of RhuT showed the typical two-domain structure of type III substrate-binding proteins. Unlike other PBPs, in the 2-heme-bound form of RhuT, pairs of Tyr and Arg residues from each domain are symmetrically located to interact with the hemes and shows a unique mechanism of heme-binding. The mutagenesis studies revealed that one Tyr from either domain is enough to retain the heme-binding property. Structural comparison of PBPs from five different species showed the diverse mode of the heme-recognition and the heme-binding cleft of PBPs can adopt an “open” state in the apo and 2-heme-bound forms, and a “closed” state in the 1-heme-bound form with unique conformational changes. Such a conformational change might adjust the interaction of the heme(s) with the residues in PBP and facilitate the transfer of the heme into the translocation channel of the importer.

2. INTRODUCTION

Iron is an essential nutrient for all life since it is involved in many important biological phenomena by virtue of characteristic chemical properties such as oxidation-reduction and reversible binding of ligands¹. Therefore, most living creatures have their own iron acquisition system. In the case of pathogens,² the iron from the heme (iron-porphyrin complex) of the host is acquired through their heme-acquisition systems. As shown in Figure 1, in the first step of the heme-uptake by Gram-negative pathogens, the heme is transferred into the periplasmic space by a TonB-dependent cell-surface heme receptor (HR),³ and then the heme is transported into the cytoplasm by an active transport system located in the inner membrane. The bacterial active heme-transport system is facilitated by the ABC (ATP-binding cassette) heme importer,^{4, 5} which is composed of a soluble periplasmic heme-binding protein (PBP), membrane-integrated heme permease subunits (TMD: trans-membrane domain), and ATPase subunits (NBD: nucleotide-binding domain). In this system, PBP shuttles the heme from the outer

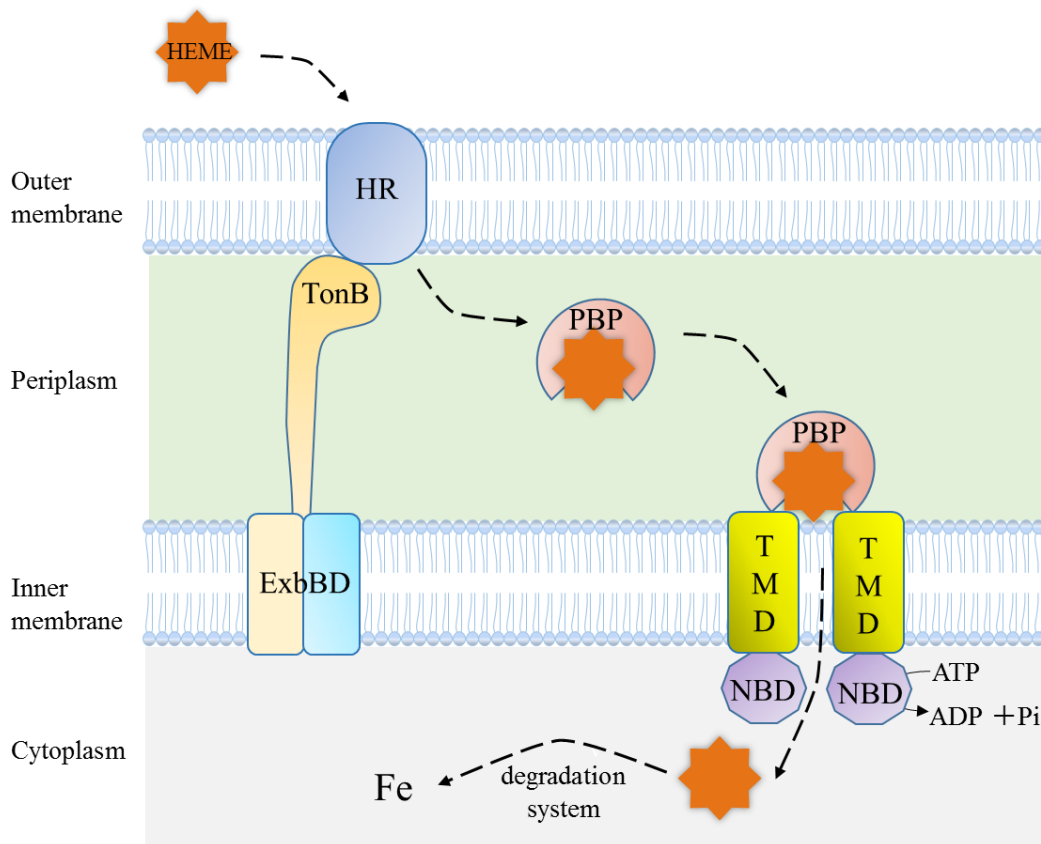


Figure 1. Heme-acquisition systems of Gram-negative bacteria. PBP captures the heme in the periplasmic space. Then the heme-bound PBP binds with the TMD of the ABC heme-importer and release the heme to TMD.

membrane to the dimeric TMD of the inner membrane. The TMD imports the heme across the inner membrane through the heme translocation channel where it undergoes structural changes coupled with ATP hydrolysis in NBD. Heme oxygenase or other heme-degrading enzymes then break down the heme imported into the cytoplasm and the iron is released (Figure 1).^{6,7}

In the ABC importer systems, the periplasmic substrate-binding proteins are known to comprise a broad family with significant selectivity and specificity.⁸ The substrate-binding proteins (SBPs) consist of N- and C-terminal domains divided by a substrate-binding cleft. The connection of these 2 domains is used to categorize the proteins into 3 classes (Figure 2).⁹ Along with the vitamin B₁₂-binding protein and the iron siderophore-binding protein, the periplasmic heme-binding protein (PBP) in the heme import system belongs to class III, in which a single α -helix connects the N- and C-domains (Figure 2C).

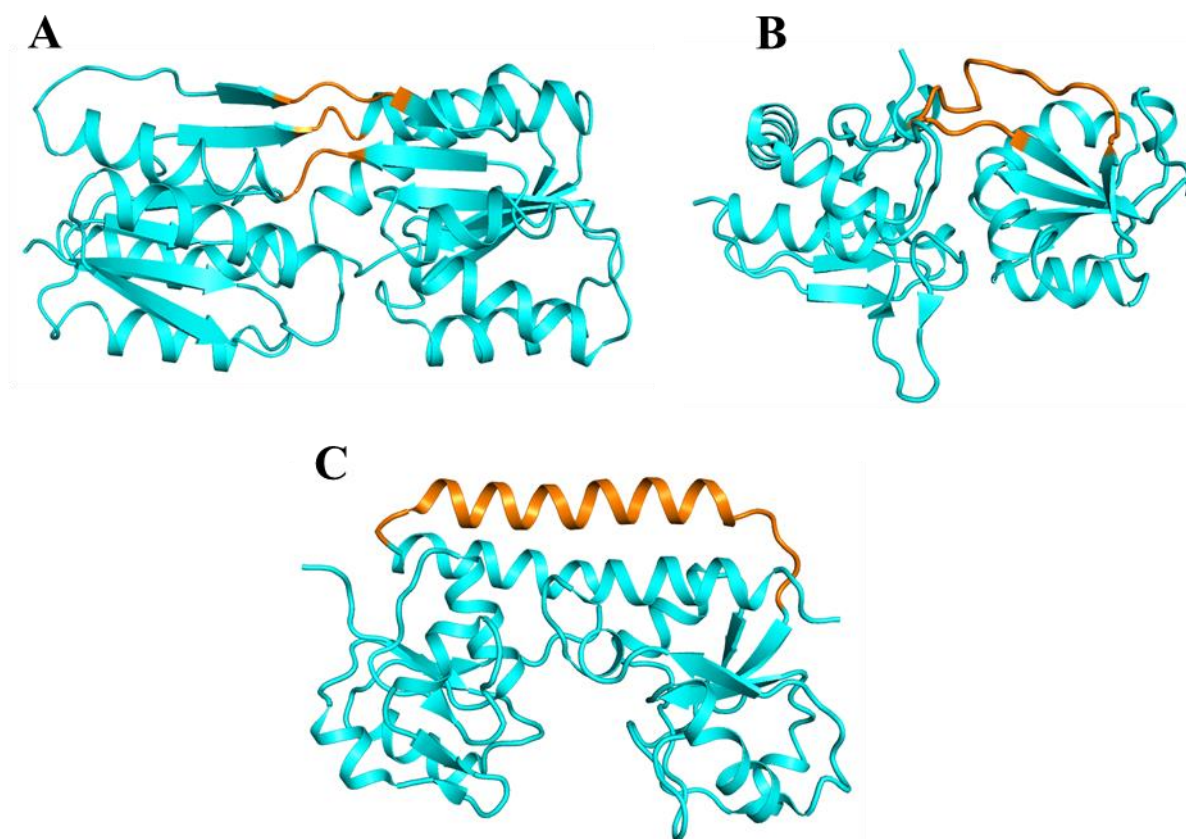


Figure 2. Classification of the substrate-binding proteins (SBPs). The different clusters of SBPs are shown with their distinct structural feature colored in orange. (A) Class I contains SBPs with three interconnecting segments between the two domains (example: RBP, PDB code: 1DRJ). (B) Class II contains SBPs with two relative short hinges (example: HisJ, PDB code: 1HSL). (C) Class III contains proteins having a single connection between the two domains in the form of a rigid helix (example: BtuF, PDB code: 1N2Z).

Previously, the crystal structures of three PBPs from Gram-negative pathogen have been reported; ShuT from *Shigella dysenteriae*,¹⁰ PhuT from *Pseudomonas aeruginosa*,¹⁰ and HmuT from *Yersinia pestis*.¹¹ These three proteins exhibit the same fold in their overall structure as other class III SBPs (Figure 3). However, it is noted that the heme binding to the cleft is different among these three crystal structures; ShuT and PhuT bind one molecule of the heme, while HmuT has two stacked hemes in its cleft. The orientation of the hemes is also different among them. Thermodynamic study of HmuT has shown that the two hemes are bound with physiologically relevant affinities ($K_D = 0.29\text{-}29\text{ nM}$).¹¹ These data suggested a new perspective of ATP-to-substrate stoichiometry because most ABC transporters are thought to transport one

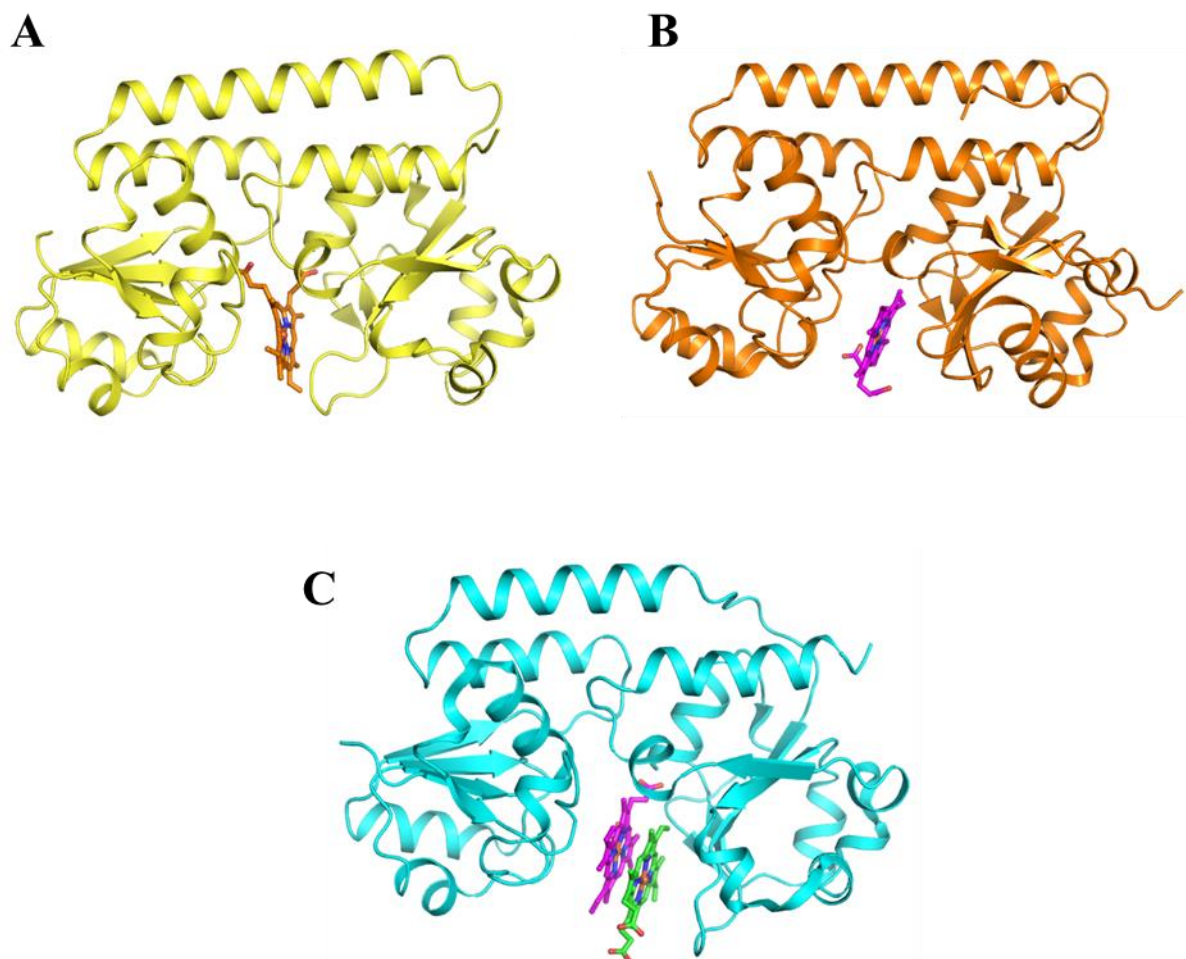


Figure 3. Crystal structures of reported PBPs. A) ShuT from *Shigella dysenteriae* (PDB code: 2R7A) and (B) PhuT from *Pseudomonas aeruginosa* (PDB code: 2R79) in 1-heme-bound form; (C) HmuT from *Yersinia pestis* (PDB code: 3NU1) in 2-heme-bound form.

substrate during the hydrolyzation of two ATP molecules, as demonstrated in OpuA.¹² It was also proposed that PBP might have adapted to acquire more than one substrate in relation to an evolutionary advantage.¹¹ However, it remains unclear how PBP changes its conformation during heme-binding, and how it transfers heme to the transporter.

Here, I present the crystal structures of a PBP (RhuT¹³) from a thermophilic Gram-negative bacteria, *Roseiflexus* sp. RS-1 in apo and heme-binding states. I used spectroscopic and biochemical techniques to understanding the heme-binding property of RhuT and performed mutagenesis studies to understand the structure-function relationship. In addition, another PBP (BhuT¹³ from *Burkholderia cenocepacia*) structures were solved by our group, and I will compare all the structures of PBPs from five species (RhuT, BhuT, HmuT, PhuT and ShuT) to understand the conservative and/or diversity in the heme-binding mechanism and how the heme is transferred from PBP to TMD.

3. MATERIALS AND METHODS

3-1 Plasmid construction and protein expression

The synthesized gene encoding residues 96-360 of RhuT was cloned into a pGEX-6P-1 vector (GE Healthcare) using *Bam*HI and *Eco*RI sites. The plasmids for mutants were generated using a QuikChange II Site-directed Mutagenesis Kit (Agilent) according to the instruction manual. The protein fused to a glutathione S-transferase (GST) tag in the N-terminal with a PreScission Protease (GE Healthcare) site was expressed in *Escherichia coli* Rosetta2 (DE3) cells (Merck Millipore). The transformed cell was picked from the LB agarose plate containing 50 µg/ml ampicillin and 34 µg/ml chloramphenicol and grown in 50 mL of LB medium at 37 °C. Then, 10 mL of pre-culture was transferred to 1 L of LB medium and overexpression of the protein was induced by 0.3 mM IPTG at an OD₆₀₀ of 0.6-0.8. The cell culture was continued for an additional 20 hours at 20 °C.

3-2 Protein purification

All of the following purification steps were performed either at 4 °C or on ice. The harvested cells expressing GST-tagged RhuT were disrupted with the French pressure cell press with Tris-buffered saline (TBS buffer consisted of 50 mM Tris-HCl pH 7.5, 150 mM NaCl). The lysate was centrifuged at 40,000 rpm for 1 hour using a Hitachi P45AT rotor with an ultracentrifuge CP80NX to remove the cell debris. The supernatant was loaded onto a column with 30 mL of Glutathione Sepharose 4B resin (GE Healthcare). The resin was washed with TBS buffer and bound protein were eluted with 10 mM reduced glutathione in 50 mM Tris-HCl pH 7.5 and 150 mM NaCl. The eluted fraction was mixed with PreScission Protease (GE Healthcare) and was dialyzed in 50 mM Tris-HCl pH 7.5, 1 mM DTT, and was again loaded into a GS4B resin column. The GST-tag cleaved RhuT sample was collected in the flow-through fraction and dialyzed in 50 mM Tris-HCl pH 8.0. Next, the sample was loaded onto an anion exchange column HiTrap Q HP (GE Healthcare) to separate the apo (90%) and heme-bound (10%) RhuT using a linear gradient of 0 to 100 mM NaCl. The protein was collected and concentrated using Amicon Ultra centrifugal filter devices (10 kDa cutoff; Merck Millipore). Purification of RhuT mutants was performed using the same procedure as WT.

3-3 Spectroscopic titration experiments

A 0.5 mM hemin stock solution was prepared as described.¹¹ 3.3 mg hemin chloride (Sigma-Aldrich) was dissolved in 500 μ L of 0.1 M NaOH, to which 500 μ L of 1 M Tris-HCl pH 8.0 was added. The solution was diluted with 20 mM Tris-HCl pH 7.5 and 150 mM NaCl to form a total volume of 10 mL. The hemin concentration was determined by pyridinehemochrome assay.¹⁴ For the absolute spectra of hemin titration, 0.5 mM hemin (in 1 μ M steps) was added to a sample cuvette containing 5.3 μ M of purified protein. To avoid the effect of free hemin, the difference spectra of hemin titration was measured by adding 0.5 mM hemin (in 1 μ M steps) to a sample cuvette containing 5.3 μ M of purified protein and to a reference cuvette containing only buffer 50 mM Tris-HCl pH 8.0. The samples were equilibrated for 10 min following the addition of each heme aliquot. The UV/Vis spectra between 300 nm and 700 nm were recorded at 20 °C using a Hitachi U-3010 spectrometer with a temperature control unit. For the mutants, the difference spectra of hemin titration were measured using the same method as WT with a protein concentration of 5 μ M.

3-4 Isothermal titration calorimetry (ITC) experiments

ITC measurements of RhuT with hemin solution were performed at 25 °C using a VP-ITC calorimeter (MicroCal Inc.). The apo-proteins were dialyzed for 10 h at 4 °C in 50 mM Tris-HCl pH 7.5 and 150 mM NaCl. The external buffer for dialysis was used to dilute the 10 mM hemin solubilized by DMSO to prepare a 0.5 mM hemin solution used for titration. DMSO was added to the protein solution (final concentration of 5%) and the protein concentrations were adjusted to 20 μ M with dialysis buffer. Prior to loading the protein and hemin solution in the calorimeter, these solutions were filtered using a PVDF syringe filter with a 0.22 μ m pore size (Merck Millipore) and were degassed using a ThermoVac apparatus (Microcal Inc.). The final hemin concentration was corrected by measuring the absorption spectra. For titration, 1.5 mL of protein was placed in the reaction cell of a calorimeter. The titration was performed by a total of 25 injections of 10 μ L of hemin solution into protein solution. The spacing time was set to 8 min for the initial 12 injections and 16 min for the latter 13 injections due to needing a longer equilibration time. For BhuT, the titration was performed by a total of 25 injections of 10 μ L into protein solution spaced at 8 min intervals until the protein sample was saturated with hemin. The experimental data were fitted to a theoretical titration curve using ORIGIN software (Microcal Inc.).

3-5 Crystallization

Apo (heme-free) RhuT was concentrated to 52.3 mg/mL and crystallized by vapor diffusion (sitting-drop) method and incubated at 20 °C using a reservoir solution containing 0.2 M MgCl₂, 50 mM glycine and 9% PEG 400. Colorless needle-shaped crystals appeared within 5 days. The crystals were cryo-protected by soaking in the solution containing 0.2 M MgCl₂, 50 mM glycine, 9% PEG 400, and 30% glycerol.

For the preparation of heme-bound RhuT crystals, purified apo (heme-free) protein (concentration: 15 mg/mL) was supplemented with a low concentration of hemin that was dissolved by DMSO (protein: hemin = 2:1) and crystallized by vapor diffusion (sitting-drop) method and incubated at 20 °C in a reservoir solution containing 50 mM MES [2-(N-morpholino) ethanesulfonic acid] pH 6.0, 0.1 M zinc acetate and 5% PEG 8000. Brown crystals appeared within 5 days. The crystals were soaked in a solution containing 50 mM MES pH 6.0, 0.1 M zinc acetate, 5% PEG 8000, 20% DMSO, and 30% glycerol.

For the preparation of the heme-bound form crystals of RhuT mutant (Y239F), purified sample (concentration: 16.5 mg/mL) was supplemented with high concentration of hemin dissolved by DMSO (protein: hemin = 1:2) and crystallized by vapor diffusion (sitting-drop) method and incubated at 20 °C in a reservoir solution containing 0.1 M MES pH 6.0, 0.2 M zinc acetate, 15% (v/v) ethanol. Brown crystals appeared within 5 days. The crystals were soaked in a solution containing 0.1 M MES pH 6.0, 0.2 M zinc acetate, 15% (v/v) ethanol, and 30% glycerol. All crystals were flash-frozen and stored in liquid nitrogen.

3-6 Optical absorption spectra

Optical absorption spectra in the crystalline state were measured using a microspectrophotometer system that consisted of a deuterium tungsten halogen lamp (Ocean Optics, DT-MINI), cassegrainian mirrors (Bunkoh-Keiki Co. Ltd.), an optical fiber, and a linear CCD-array spectrometer (Ocean Optics, SD2000). The absorption spectra were corrected for the air blank baseline and dark reference. The crystals were maintained at 100 K via a nitrogen gas stream.

3-7 X-ray diffraction measurements, phase determination, and structure refinement

X-ray diffraction data were collected using the BL32XU of SPring-8, Japan and were processed using the HKL2000 and CCP4¹⁵ programs. The data collection and refinement statistics are shown in Table 1. The initial phases for apo and 2-heme-bound RhuT crystals were obtained via MR. The structure of HmuT (PDB code 3MD9) was used as a search model for 2-heme-bound RhuT data using the Phaser program.¹⁶ The obtained phase was improved by DM¹⁷ and was used to build the automated model by ARP/wARP.¹⁸ The apo RhuT phase was determined via MR using the 2-heme-bound RhuT model. The initial models were subjected to multiple rounds of manual rebuilding using Coot¹⁹ followed by a restrained refinement using Refmac5.²⁰ The structure refinement data are shown in Table 1.

3-8 Resonance Raman spectroscopy

The resonance Raman (RR) spectra were recorded using a single polychromator (Jovin Yvon, SPEX750M) equipped with a liquid nitrogen-cooled CCD detector (Roper Scientific, Spec 10:400B/LN) using the 405.1 nm emission line from a diode laser (Ondax, SureLock™ LM-405-PLR-40-2). Measurements were carried out at room temperature using a spinning cell (2,000 rpm) with a diameter of 8 mm. The incident light through a circular aperture (~1 mm in diameter) was focused using a lens with a focal length of 200 mm, and its power was adjusted to 5 mW at the sample point. The scattered light was collected at right angles to the incident light and focused on the entrance slit (150 μm) of the polychromator. Indene was used as a reference for the spectral calibration. The UV–visible absorption spectra were recorded before and after the RR experiments in order to verify that the samples were not altered by their exposure to the laser beam. A protein sample at a final concentration of 25 μM was prepared in 50 mM Tris-HCl pH 8.0. The hemin stock solution was prepared dissolving the hemin chloride in DMSO.

Table 1. X-ray data collection and refinement statistics

	WT Apo	WT 2-heme-bound form	Y239F 2-heme-bound-form
Data collection			
Beamline (SPring-8)	BL32XU	BL32XU	BL32XU
Space group	$P3_121$	$C222_1$	$C222_1$
Wavelength (Å)	1.0	1.0	1.0
Cell dimensions			
a, b, c (Å)	71.0, 71.0, 78.2	67.3, 86.3, 118.8	67.8, 86.6, 118.6
Resolution (Å) ^a	50 – 2.4 (2.44 – 2.40)	50 – 2.0 (2.03 – 2.0)	50 – 2.0 (2.03 – 2.0)
Observed reflections	115,667	190,084	230,107
Unique reflections	9,202	23,911	20,998
R_{sym} (%) ^{a,b}	9.8 (50.1)	11.4 (54.4)	8.7 (71.9)
Average $I/\sigma(I)$ ^a	26.5 (3.4)	14.7 (2.4)	28.2 (2.7)
Completeness (%) ^a	99.3 (94.5)	99.8 (97.8)	99.6 (99.2)
Redundancy ^a	12.6 (7.0)	7.9 (7.1)	11.0 (10.0)
Refinement			
R_{work} (%) ^c	18.6	18.3	18.8
R_{free} (%) ^c	25.5	22.4	22.5
No. of residues	265	276	268
No. of waters	46	126	133
R.m.s.d bond (Å)	0.009	0.016	0.018
R.m.s.d angles (°)	1.31	1.83	2.04
Ramachandran plot ^d			
Favored region (%)	97.7	98.5	96.3
Outlier regions (%)	0.0	0.0	0.0

^a Values in parentheses are for the highest-resolution shell.

^b $R_{\text{sym}} = \sum_{hkl} \sum_i |I_i(hkl) - \langle I(hkl) \rangle| / \sum_{hkl} \sum_i I_i(hkl)$, where $\langle I(hkl) \rangle$ is the average intensity of i observations.

^c $R_{\text{work}} = \sum_{hkl} |F_{\text{obs}}(hkl) - F_{\text{calc}}(hkl)| / \sum_{hkl} F_{\text{obs}}(hkl)$, where F_{obs} and F_{calc} are the observed and calculated structure factors, respectively. R_{free} was calculated with 5% of the reflections.

4. RESULTS

4-1 Protein purification and crystallization

Purified protein (~28 kDa) was obtained after affinity chromatography (Glutathione Sepharose 4B resin). Further, the apo and heme-bound forms were separated by anion-exchange chromatography.

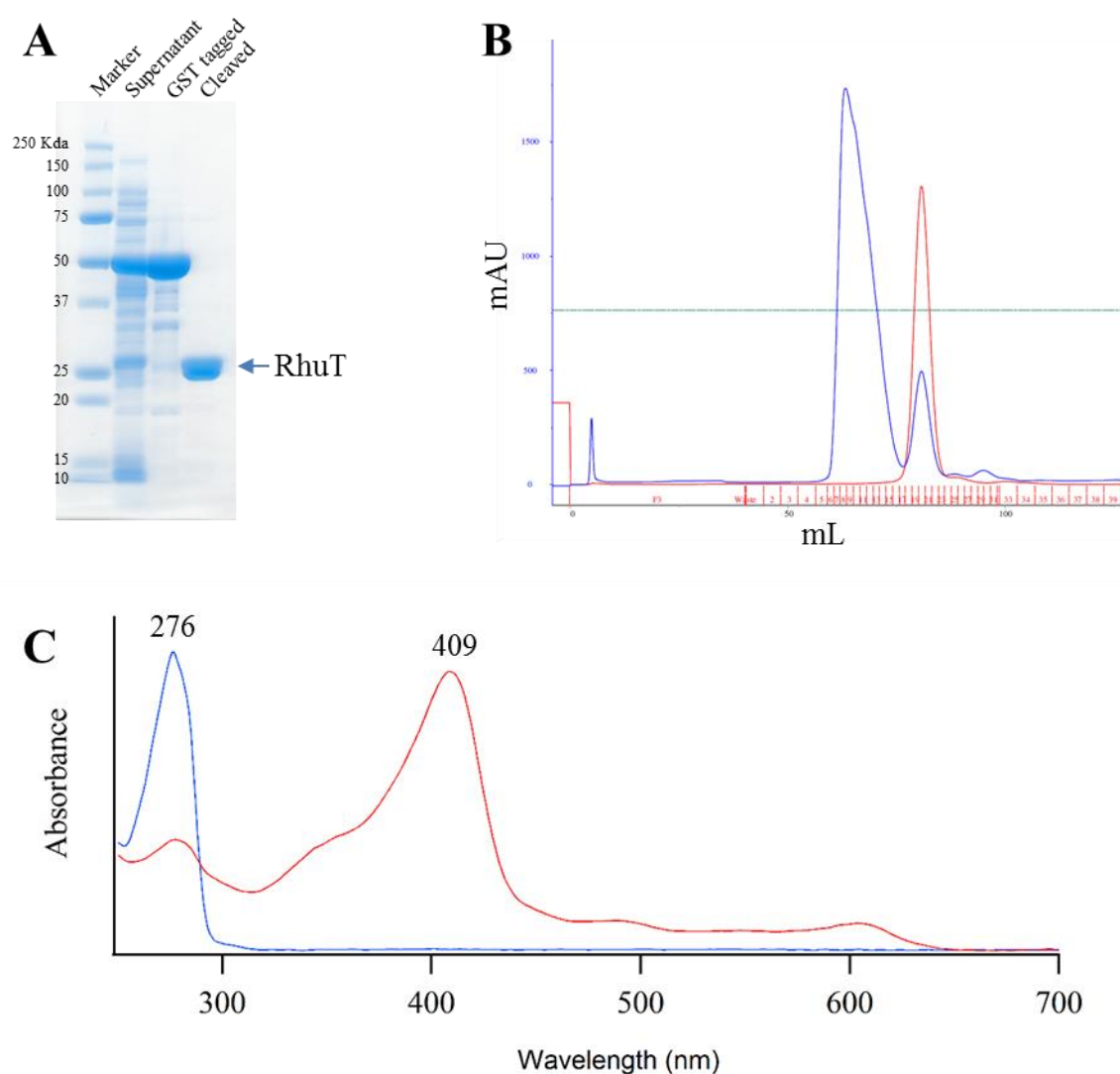


Figure 4. Protein purification profile. A) SDS-PAGE after affinity chromatography. B) Anion-exchange chromatography result. The blue colored line represent the absorbance at 280 nm and red line represents the absorption spectrum at 410 nm. C) UV-Vis absorption spectra of separated apo (blue) and heme-bound (red) forms of RhuT.

The purified sample of apo (heme-free) RhuT was concentrated to 52.3 mg/mL and crystallized by vapor diffusion (sitting-drop) method (Figure 5).

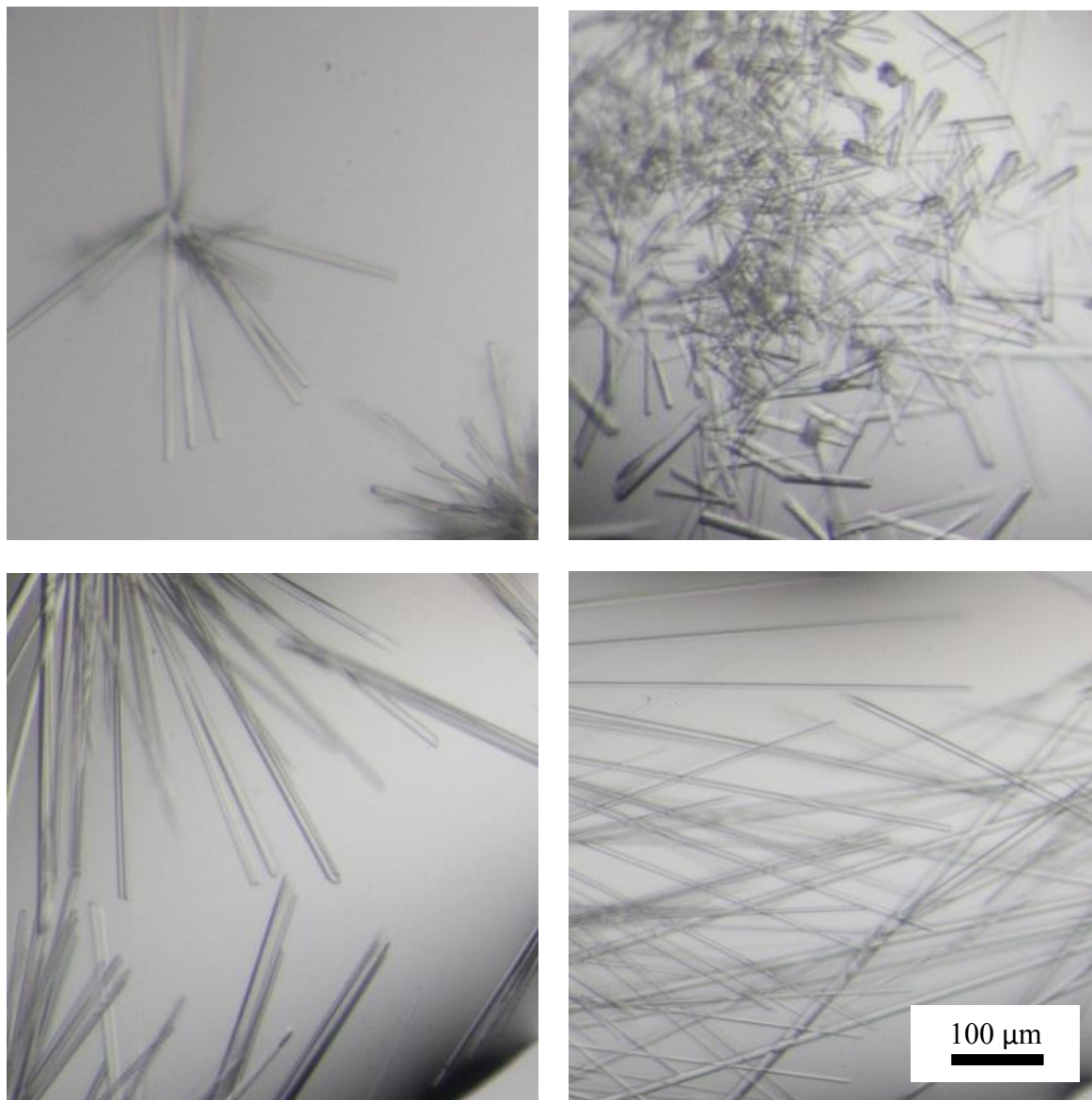


Figure 5. Apo form crystals. The crystals were appeared within five days of crystallization by vapor diffusion (sitting drop) method.

4-2 Crystal structure of apo form

The crystal structure of the apo (heme-free) form of RhuT was determined at resolutions of 2.4 Å (Figure 6). The overall folds of RhuT share common structural features with class III substrate-binding proteins,⁹ which consists of two topologically similar domains (N-domain and C-domain) and the two domains are connected by a rigid α -helix (connecting helix) as an inter-domain linker.

Each domain has a β -sheet surrounded by few short α -helices, and there is a loop region between each domain and rigid connecting helix, which is important for the domains motion. The cleft between the N- and C-domain serves as the heme-binding site. One Glu residue is present on the surface of each domain (E147 in the N-domain and E282 in the C-domain), and these are well conserved in all PBPs (Figure 7). It has been shown that the interaction of these Glu of PBP and the conserved Arg residues on the periplasmic surface of the TMD of the ABC heme importer creates the salt bridge to form the stable complex.^{11, 21}

The structure of the heme-binding cleft of apo RhuT is illustrated in Figure 6B. In the heme-binding cleft of apo RhuT, some hydrophilic (Y140, Q141, R142, R143, Y239, R241) and hydrophobic (L295, F276, L334) side chains and several water molecules are present. Of these residues, the Y140 and R142 are conserved residues in most PBPs, as shown in the sequence alignment of PBPs from five species (Figure 7). On the other hand, the residues from the C-domain side are not well conserved.

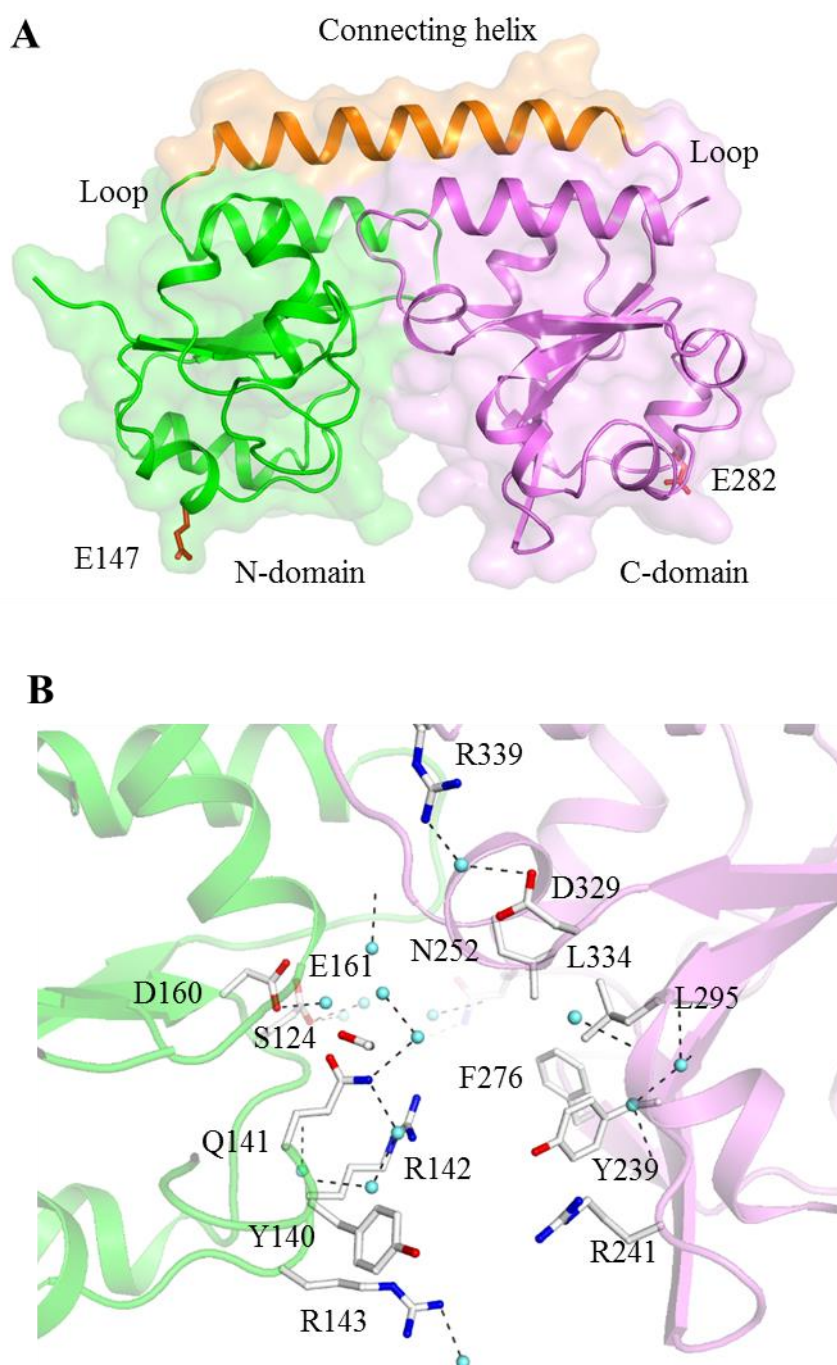


Figure 6. The overall structure and heme-binding cleft in apo form. (A) Apo RhuT structure shows an open cleft between the N-domain (green) and the C-domain (violet). The connecting helix between two domains is colored by orange. (B) The heme-binding cleft shows the residues and water molecules present in the cleft. Residues in the cleft are showing as stick (white), water molecules as sphere (cyan) and dashed line represents the corresponding H-bonds.

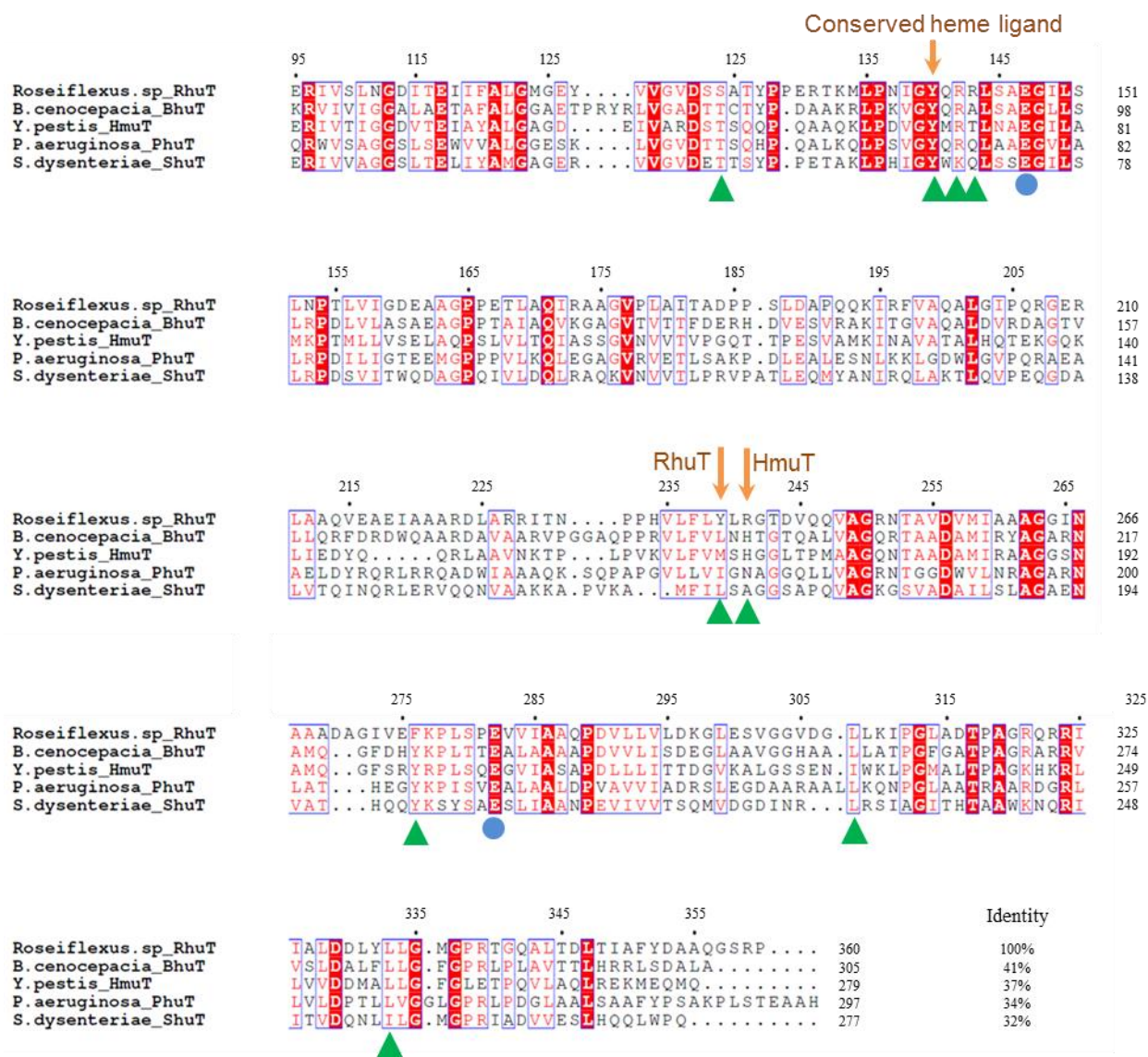


Figure 7. Sequence alignment of PBP homologues from representative organisms. The residues in the heme binding clefts of RhuT are indicated by green triangles. Ligands for the heme iron are marked by arrows, and two conserved glutamate residues to interact with TMD are marked by blue circles. Percentages of sequence identity are shown in the end of the last line.

4-3 Heme-binding in solution

To examine the binding of heme to RhuT, the UV/visible absorption spectral changes upon titration with hemin into protein solution was measured. The absolute spectra (Figure 8) showed two-step spectral change. The first peak appeared at 409 nm and the second peak at 379 nm. To avoid the free hemin effect, the difference spectra were measured (Figure 9). The difference spectra in this titration experiment showed a clear two-step spectral changes. At first, the peak at 413 nm was increased with the increment of hemin concentration until the hemin concentration equivalent to the protein concentration. Further addition of hemin resulted in a new peak appeared and increased at 373 nm with a concomitant decrease of the peak at 413 nm. Considering the protein to hemin ratio, the peak at 413 nm is assigned as the 1-heme-bound form and that at 373 nm as the 2-heme-bound form. These spectral observations indicated that, in solution, the cleft of RhuT had the ability to accommodate 2 heme molecules sequentially

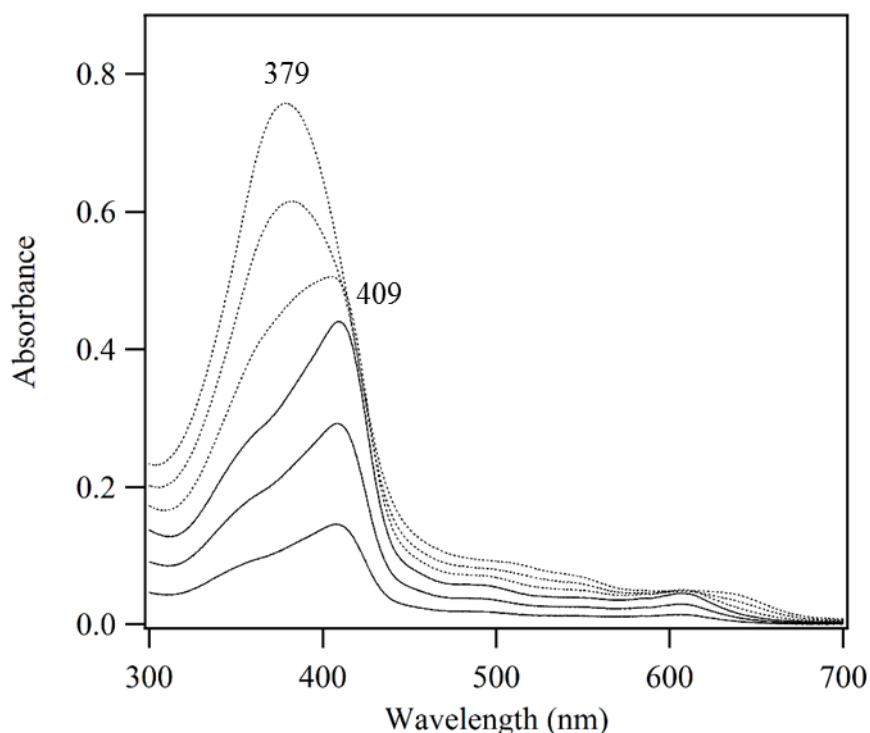


Figure 8. The UV/vis absorption absolute spectra in the hemin titration. Spectrophotometric titrations were performed by stepwise addition of hemin ($1 \mu\text{M}$ steps) to the solution of RhuT ($5.3 \mu\text{M}$) in buffer (50 mM Tris, $\text{pH } 8.0$, 150 mM NaCl). The solid line represents the spectra with lower hemin concentration to protein concentration and dotted line represents the spectra with higher hemin concentration to protein concentration. For clarity, few spectra are presented here.

depending on the heme concentration. The 1-heme-bound form was isolated until the addition of an equimolar amount of heme and then followed by the 2-heme-bound form, as shown in the inset of Figure 9, possibly because the affinity for the second heme-binding to RhuT might be much lower than that for the first heme.

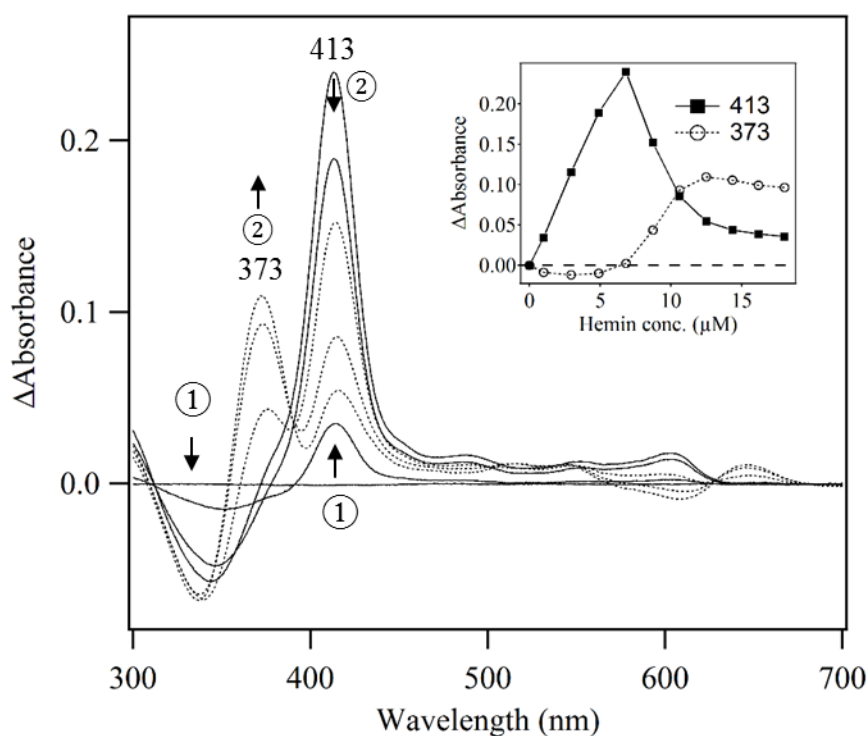


Figure 9. The UV/vis absorption difference spectra in the hemin titration. Spectrophotometric titrations were performed by stepwise addition of hemin to RhuT (5.3 μ M) in buffer (50 mM Tris-HCl, pH 8.0, 150 mM NaCl). A reference was made for the measurement of the difference spectra by addition of the same amount of hemin to the buffer. The solid line represents the spectra with lower hemin concentration to protein concentration (molar ratio less than 1:1) and dotted line represents the spectra with higher hemin concentration to protein concentration (molar ratio higher than 1:1). For clarity, few spectra are presented here. The changes of the spectral peaks are marked by arrows, and their orders are indicated by the numbers in the circles. The differences at 413 and 373 nm following the incremental addition of hemin to RhuT are plotted in the inset.

4-4 Thermodynamic analysis

Isothermal Titration Calorimetry (ITC) was used to characterize the interaction between the RhuT and heme. The ITC data (Figure 10) showed a very unique isotherm that was characterized by three phases with alternating enthalpies, indicating multiple populations of heme-bound to RhuT. Because this data was complex, the analysis using either two sets of site models or two sequential models (Figure 11) was unsuccessful.

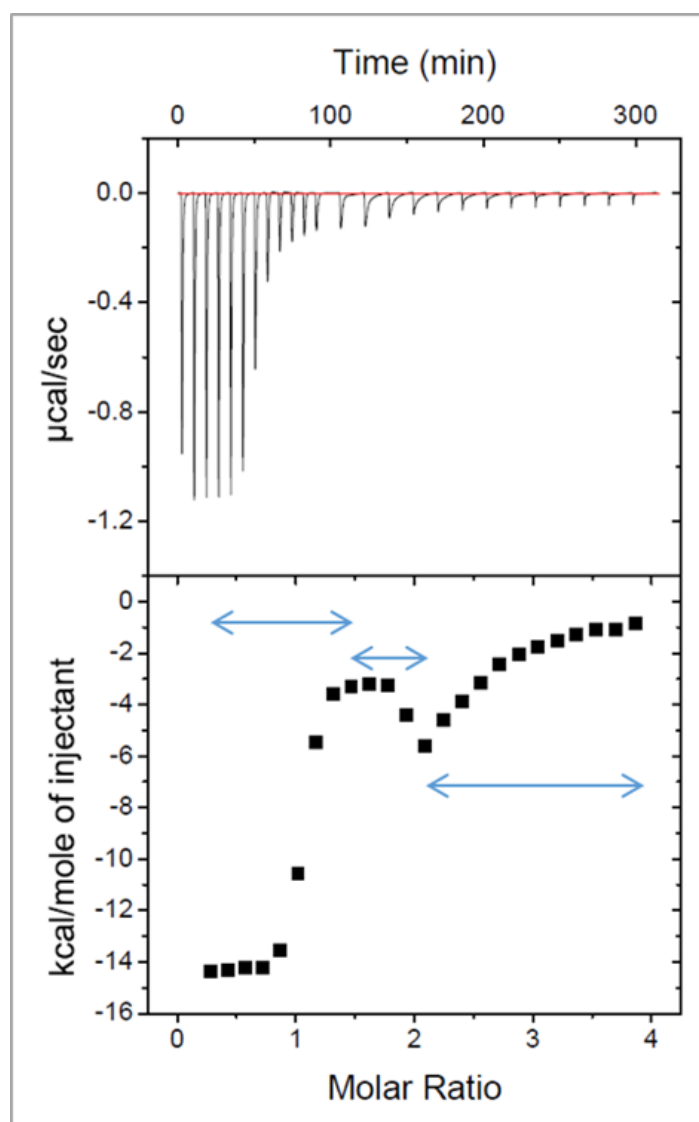


Figure 10: Isothermal titration calorimetry of the heme binding to RhuT. Titration of 20 μM RhuT with 0.4 mM hemin. Top panel, differential heating power versus time. Lower panel, integrated and normalized heat of reaction versus the molar ratio. Experimental data are shown by black squares.

The UV/vis difference spectra of RhuT showed that until the molar ratio of protein and hemin 1:1, only 1-heme-bound form appeared and in higher hemin concentration 2-heme-bound form appeared and saturated around the ratio 1:2 of protein: hemin (Figure 9). In ITC data, only one phase was observed until the protein to hemin ratio 1:1 (spacing time of 8 min), but it was unusual that around molecular ratio of 1:2, RhuT required a very long equilibration time (spacing time of 16 min) between each injection for the precise measurement and two phases were observed. The long equilibration time indicates the large conformational changes during heme binding to RhuT. Although the thermodynamic parameters could not be obtained for RhuT, comparison of the ITC data of BhuT¹³ and HmuT¹¹ (Figure 11) revealed the diverse modes and complexity of the heme-recognition by PBPs, which likely reflects the difference in the residue type and number of the heme ligand, and their solvent structures in the heme

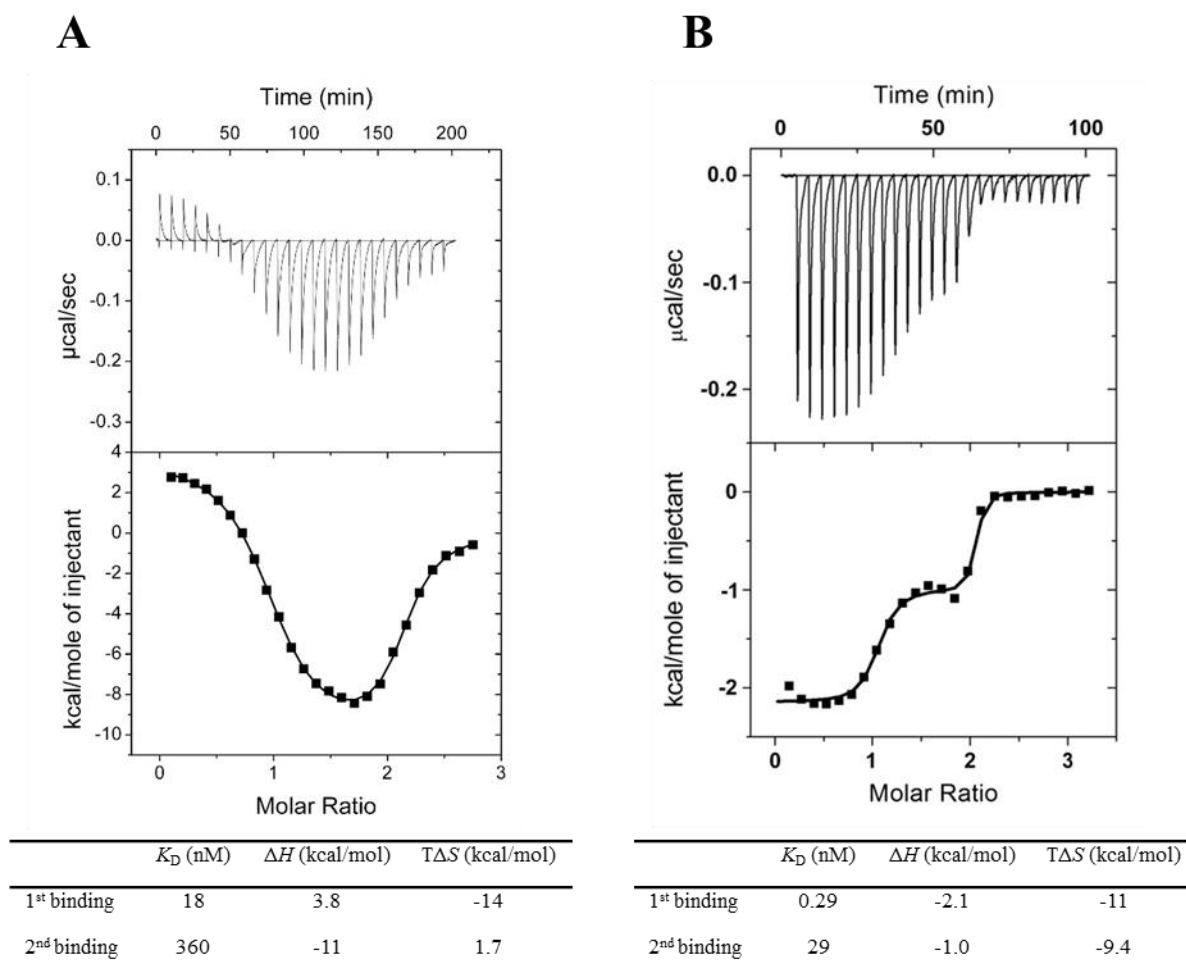


Figure 11. ITC data for homologues. (A) ITC data of BhuT showing two site binding model and (B) ITC data of HmuT fitted by two sequential binding model (Modified from Mattle, D., Zeltina, A., Woo, J. S., Goetz, B. A., Locher, K. P., *J. Mol. Biol.* **404**, 220-231 (2010)). The thermogram of HmuT also shows valley at molecular ratio of 1:2, indicating the similarity with RhuT.

cleft.

4-5 Crystal structure of heme-bound form

The purified apo form (heme-free) of RhuT was supplemented with hemin for the preparation of heme-bound form crystals (Figure 12), and crystallized by vapor diffusion (sitting-drop) method.

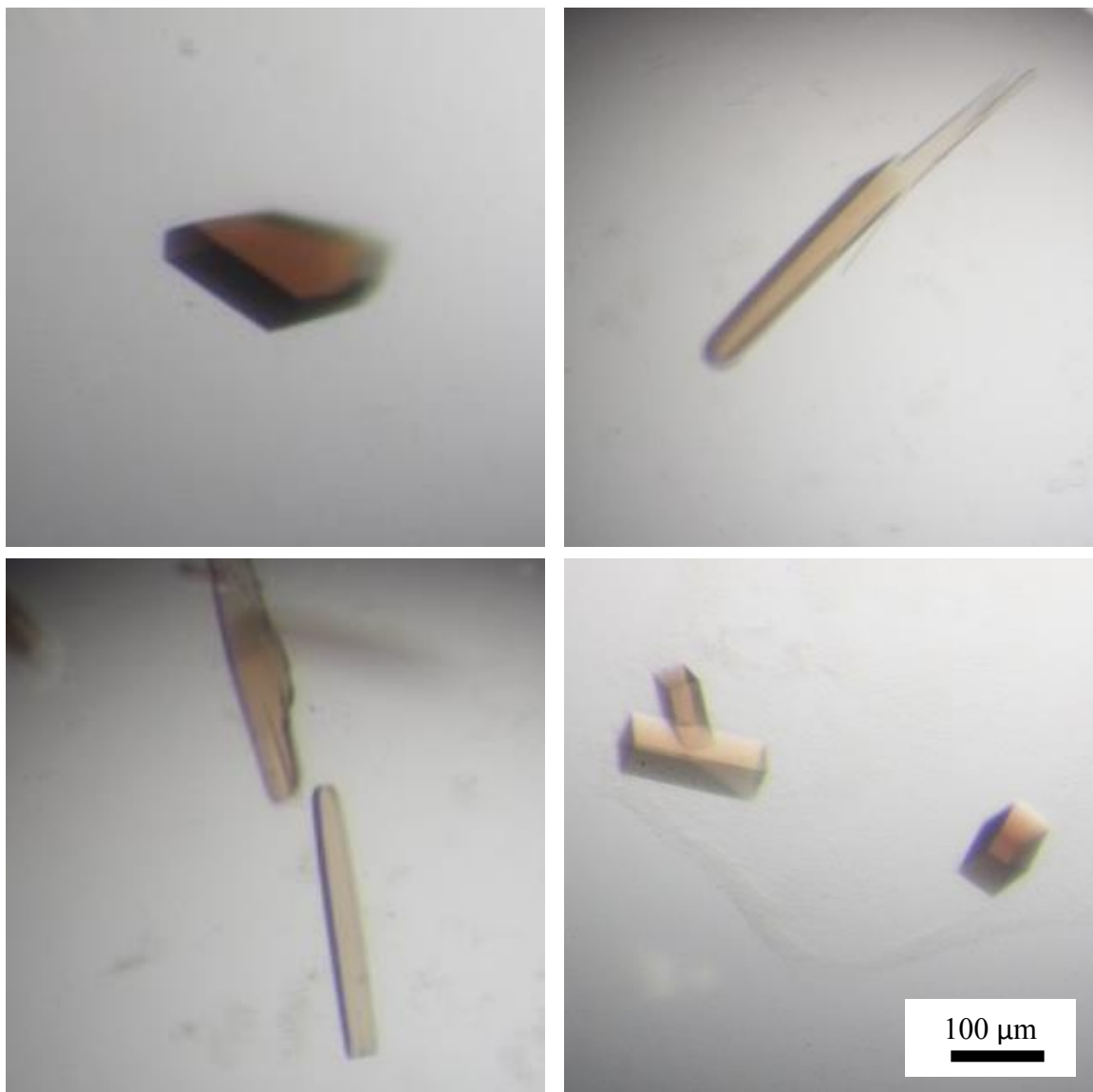


Figure 12. Heme-bound form crystals. The crystals appeared within five days of crystallization by vapor diffusion (sitting drop) method.

The optical absorption spectra in the crystalline form clearly showed that the RhuT crystals of the 2-heme-bound form were obtained and showed the solet peak at 373 nm (Figure 13). The crystal structures of the 2-heme-bound form at the resolution of 2.0 Å is shown in Figure 14. Until now, any crystal of 1-heme bound form of RhuT has not been obtained, after screening many crystallization conditions with different protein: hemin ratios. In the 2-heme-bound form (Figure 14), the two heme molecules are stacked with a Fe-Fe distance of 4.5 Å and a heme - heme plane distance of 3.6 Å. The propionates of both heme molecules point toward bulk solvent. The Y140 phenolate was coordinated to the heme_N iron as the fifth axial ligand and interacted with the R14 and Q141 via a hydrogen bonds. The guanidyl group of R143 interacted with two propionates of the heme_N. It is interesting that the coordination of heme_C is very similar to that of heme_N, where the phenolate of Y239 coordinates with the iron and interacts with the R241 via hydrogen-bond. Some hydrophobic residues L295, F276, and L334 are also interacting with the heme_C from a distance range of 3.4 to 4.0 Å.

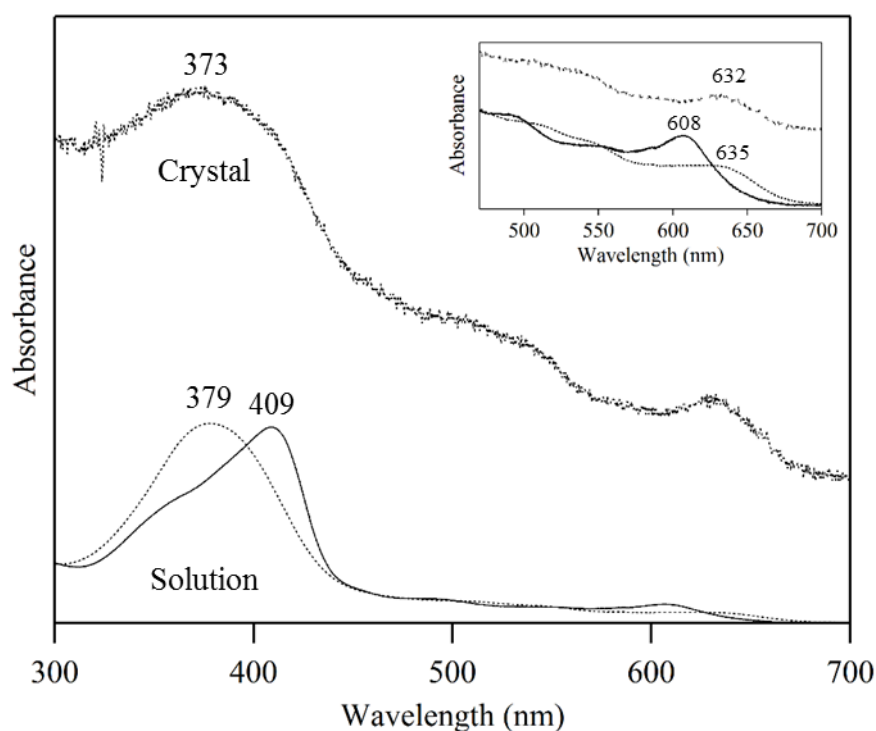


Figure 13. Absorption spectra of RhuT in crystal and solution. Spectra of 2-heme-bound form crystal of RhuT are compared with the spectra of 1-heme-bound (solid line) and 2-heme-bound (dotted line) forms in solution. Absorbance are shown in an arbitrary scale. The inset shows an enlarged portion of the visible region. Presence of the free hemin in solution affects the peak wavelength of the spectra of the 2-heme-bound form.

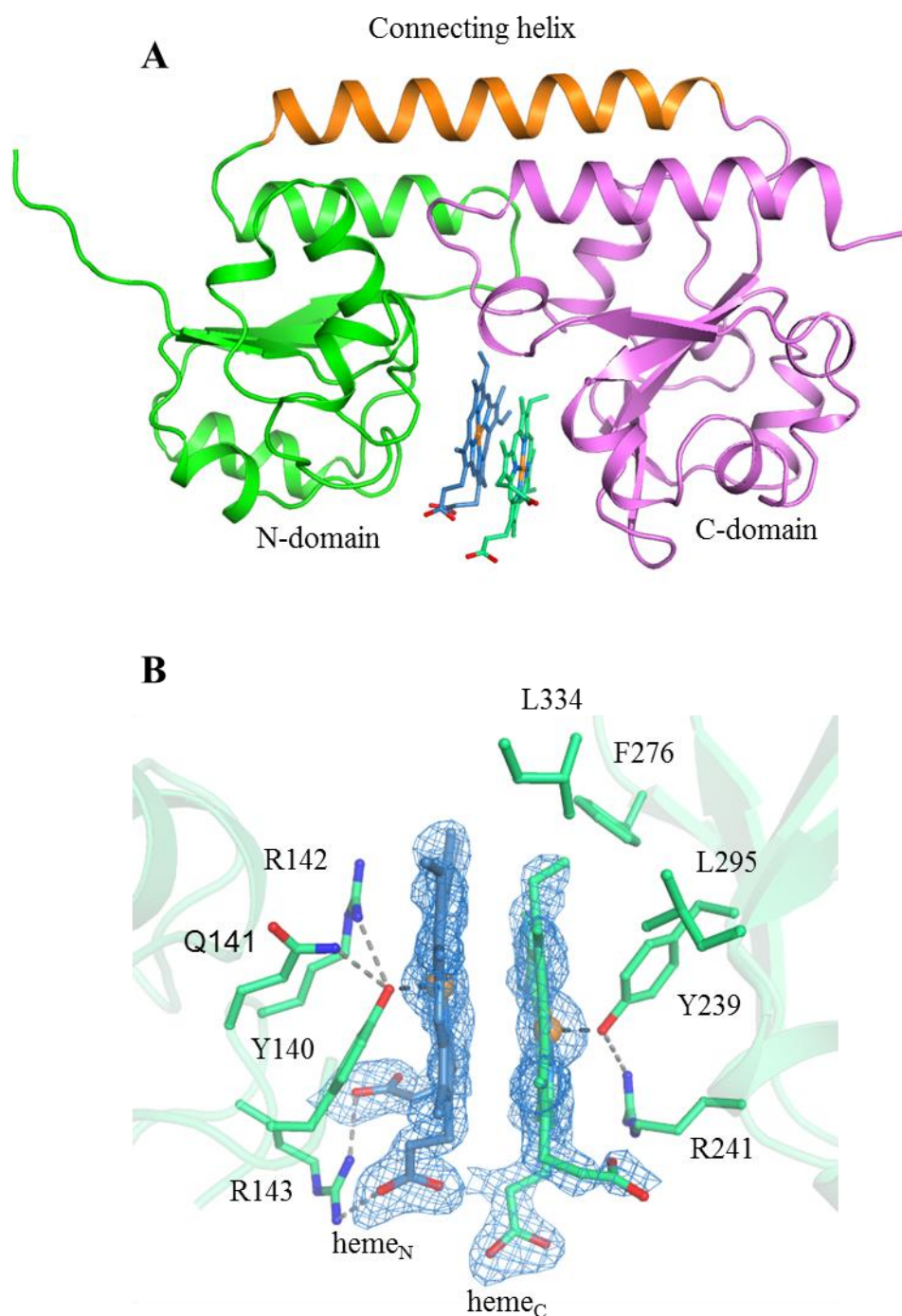


Figure 14. Crystal structure of the heme-bound form. (A) The overall structure of RhuT in the 2-heme-bound form, (B) the heme-binding cleft in the 2-heme-bound form showing one heme bound to the N-domain as heme_N and the other heme bound to the C-domain as heme_C. The $F_o - F_c$ omit maps around the hemes are shown at the 2.5σ level.

4-6 Comparison of apo and heme-bound forms

Although the overall structures of the apo and 2-heme-bound forms were similar, the superposition of these two structures (Figure 15 A) showed that the relative positions of the N- and C-domains were substantially changed upon the heme binding to the apo form. The heme binding cleft becomes wider to accommodate the two hemes compare to the apo form structure. As the connecting helix is rigid, the two domains motion should be achieved by the loop region (situated between each domain and connecting helix) to accommodate the hemes.

In the heme-binding cleft (Figure 15 B), large conformational changes were observed for the heme ligand Y140 in N-domain and R241 in the C-domain. These large conformational changes enable the interaction between Tyr and Arg in each domain. The Tyr and Arg pair is almost conserved in all reported PBPs and is proposed to be important residues for the effective heme-capturing mechanism by PBP. The relative position of the other interacting residues (Q141, R142, Y239, F276, L295, and L334) in the heme-binding cleft were also changed significantly during heme-binding.

The residues in cleft showed comparatively higher *B*-factor in the apo form structure (figure not shown) and show significant conformational changes during heme-binding. Several water molecules appeared in the heme cleft of the apo form (Figure 6B), but most of them were expelled upon binding of hemes.

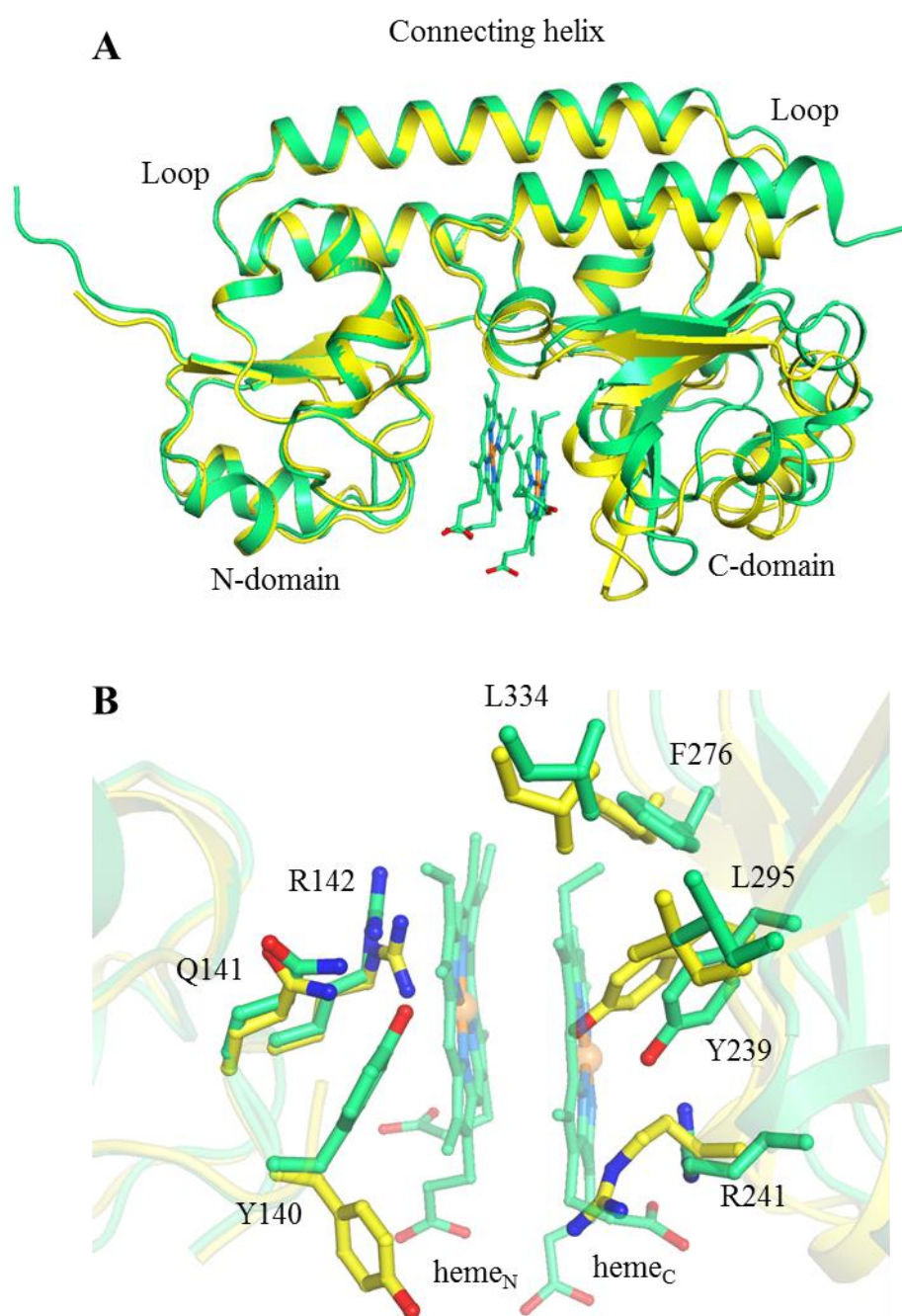


Figure 15. Comparison of apo and 2-heme-bound forms structures of RhuT. (A) Superimpose of the apo form (colored by yellow) and the 2-heme-bound form (colored by green) structures. The $C\alpha$ atoms of the N-domain were used for fitting calculation. (B) The heme-binding cleft showing the relative position of the residues in the apo (yellow) and in 2-heme-bound (green) forms. The $C\alpha$ atoms of the connecting helix were used for fitting calculation. The residues are showing as stick model.

4-7 Heme environmental structure in solution

The resonance Raman (RR) spectra of RhuT was measured to confirm that the unique coordination structure of RhuT in the 2-heme-bound form observed by X-ray crystallographic analysis is not the artifact of the packing effect in the crystal and to see the coordination structure of the 1-heme-bound form. In the UV-visible spectra (Figure 9), the 1-heme-bound form was observed in lower hemin concentration (< protein concentration) and 2-heme-bound form appeared in the higher hemin concentration (> protein concentration).

In the RR spectra (Figure 16), the ν_4 band which is a characteristic of porphyrin π^* electron density and iron oxidation state was observed near 1370 cm^{-1} in both lower and higher concentrations of the hemin to protein and is indicative of ferric heme. The ν_3 band is the marker band for the heme coordination and the spin-state of the heme. In lower hemin concentration to protein, the ν_3 band appeared at 1474 cm^{-1} (Figure 16A), indicating the presence of six-coordinate high-spin (6cHS) heme in the 1-heme-bound form. Possible candidates for the sixth ligand are H_2O , OH^- or the phenol group of Tyr 239. Water is more reasonable as there is no evidence of heme binding with two electronegative residues.

On the other hand, in the higher hemin concentration to protein (Figure 16B), the ν_3 bands shifted to 1489 cm^{-1} compares to the lower hemin concentration (1474 cm^{-1}), showing the presence of five-coordinate high-spin (5cHS) heme in the 2-heme-bound form, which is consistent with the crystal structure of the 2-heme-bound form (Figure 14).

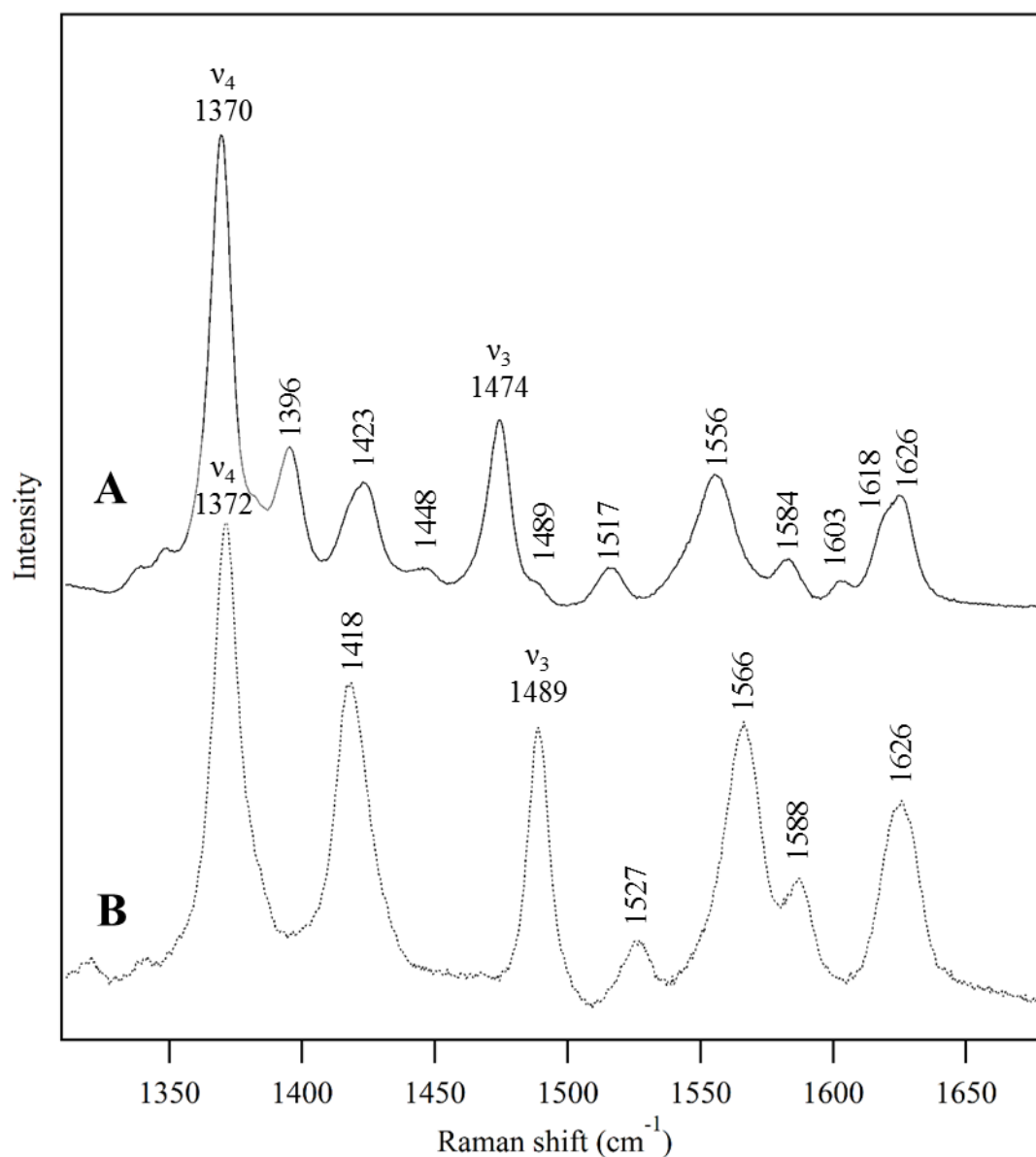


Figure 16. Resonance Raman (RR) spectra of RhuT with addition of hemin. The high-frequency region of RR spectra of RhuT after adding the hemin solution. (A) The spectra of 25 μM RhuT with the lower hemin concentration (20 μM) and (B) the spectra of 25 μM RhuT with the higher concentration of hemin (52 μM). The DMSO was used to dissolve the hemin and showed the bands in the 1418-1423 cm⁻¹ region.

4-8 Mutagenesis studies

To understand the structure-function relationship, the site-directed mutagenesis was performed targeting the residues interacting with the two hemes (Figure 17). The following eight mutants including single and double mutants were prepared using the site-directed mutagenesis method for mutagenesis studies:

- Y140F and Y239F: The ligands of the hemes
- R142V and R241V: Residues interacting with the two Tyr ligands
- Y140F/R142V and Y239F/R241V: Two Tyr-Arg motifs in the cleft
- F276A and L295A: Hydrophobic residues which interact with the heme_C

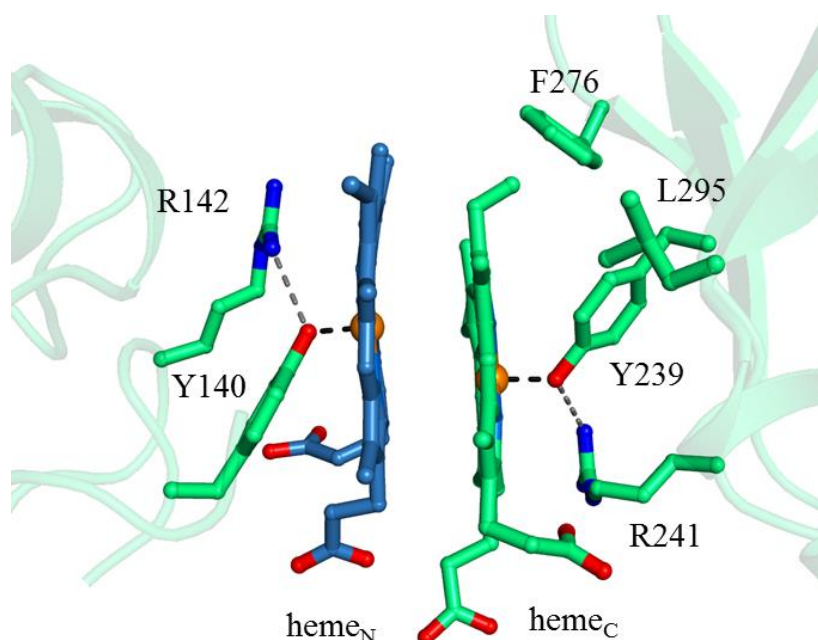


Figure 17. Targeting residues in the heme-binding cleft for mutagenesis studies.

4-8-1 Heme-binding property of mutants

To examine the heme-binding property of RhuT mutants, UV-visible absorption spectra of RhuT mutants in the hemin titration were compared with those of WT (Figure 9). The difference absorption spectra of hemin titration experiments of mutants showed a significant difference in the absorption peak positions as well as in the overall pattern of the absorption spectra.

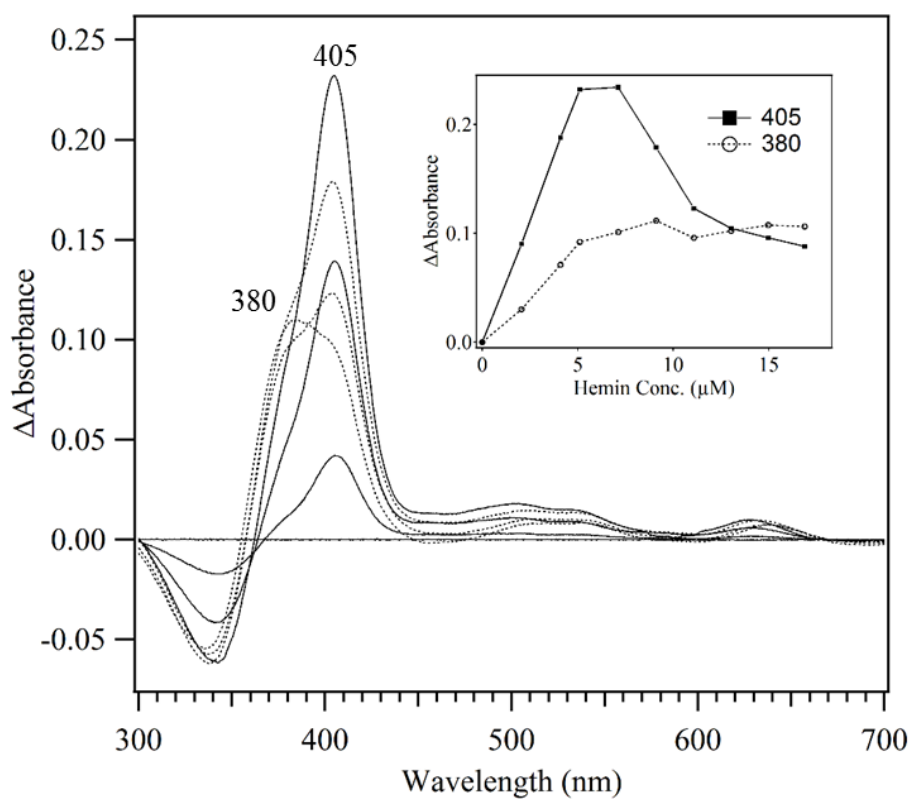
Tyrosine and Arginine mutants (Y140F, Y140F/R142V, Y239F, Y239F/R241V, R142V, and R241V):

The UV-visible difference absorption spectra showed two peak positions for all of these mutants. In the case of Y140F and Y140F/R142V mutants, two common peaks appeared at 405 nm and 380 nm (Figure 18 A and B). In both mutants, the peak maximum at 380 nm reached in hemin concentration 8-9 μM , whereas the peak maximum at 405 nm reached in hemin concentration 7 μM or 4 μM for Y140F and Y140F/R142V mutants respectively. In the case of Y239F and Y239F/R241V mutants, one common peak appeared at 385 nm and another peak at 406 or 404 nm respectively (Figure 18 C and D). In both mutants, the peak maximum at 385 nm reached in hemin concentration 14 μM , whereas in 406 or 404 nm, the peak maximum reached in the hemin concentration 8 μM or 4 μM for Y239F and Y239F/R241V mutants respectively. In the case of R142V mutant, two peaks appeared at 405 and 375 nm whereas for R241V mutants at 407 and 377 nm (Figure 18 E and F). In both mutants, the peak maximum at 375 or 377 nm reached in hemin concentration 10 μM , whereas in 405 or 407 nm, the peak maximum reached in a hemin concentration of 6 μM . Compared with the spectral change of WT (Figure 9), the first peak of these mutants shifted from 413 nm to a range of 404-407 nm, but the second peak varied widely within a range of 375-385 nm (Figure 18 A-F). For both single and double mutants (Y140F and Y140F/R142V) of N-terminal heme ligands, the second peak shifted to 380 nm, whereas it shifted to 385 nm for C-terminal heme ligand mutants (Y239F and Y239F/R241V). The two Arg mutants (R142V, R241V) showed a shift to 375-377 nm as observed in WT at 373 nm. All of the single and double mutants of these four residues (Y140F, Y140F/142V, Y239F and Y239F/R241V) of RhuT showed two peaks of the absorption spectra, which indicate that they retain the 2-heme-binding ability. In the case of WT (Figure 9), in lower hemin concentrations, only the 1-heme-bound form appeared and then the 2-heme-bound form appeared in higher hemin concentrations, whereas all these mutants showed a mixture of 1-heme- and 2-heme-bound forms even at lower hemin concentrations.

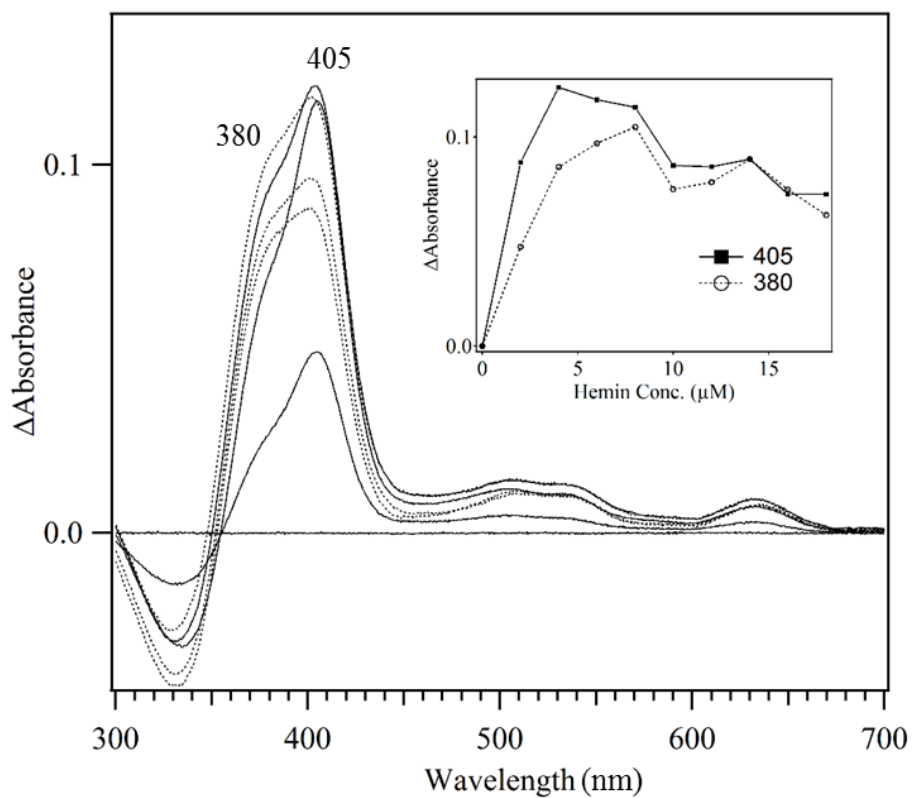
Mutants of hydrophobic residues (F276A and L295A):

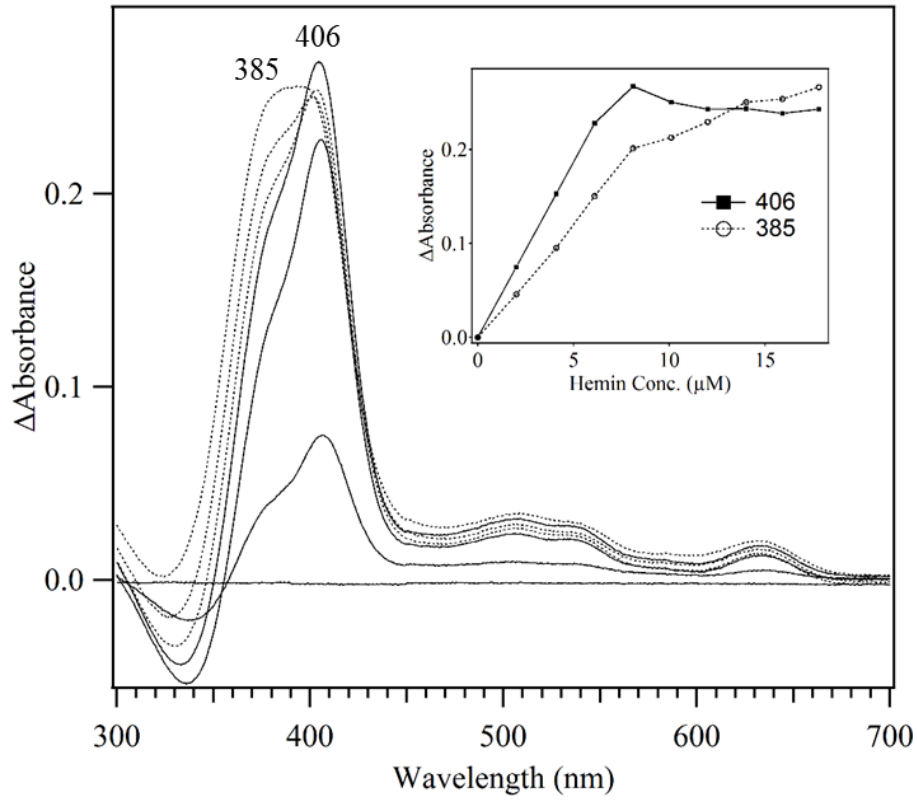
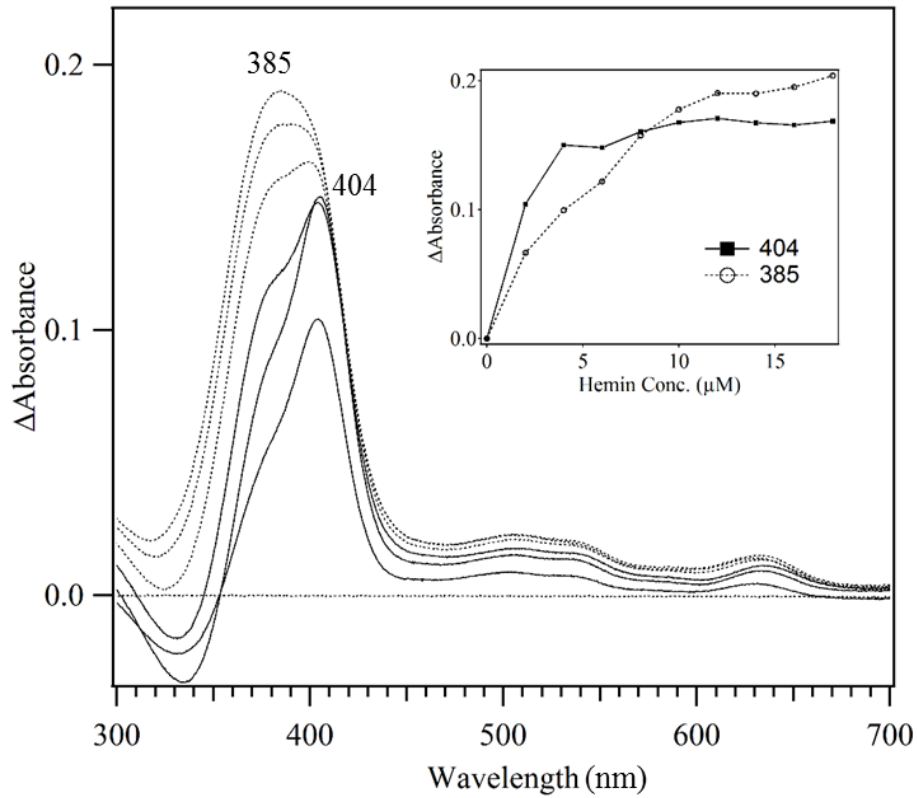
The structure shows that the hydrophobic residues (F276 and L295) interact with the heme_c (Figure 17). Both mutants (F276A and L295A) show (Figure 18 G and H) similar spectra of WT (Figure 9) indicating the less effect on the heme-binding environment compare to those interacting either with the heme or the heme ligands by hydrogen-bonds (Tyr and Arg).

A **Y140F**

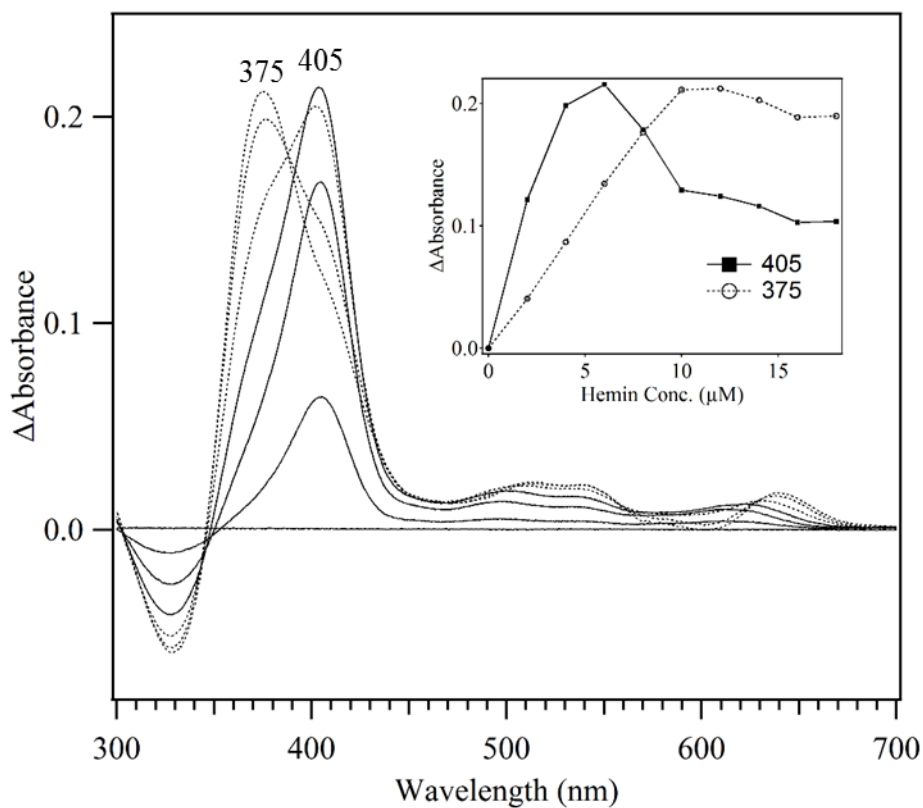


B **Y140F/R142V**

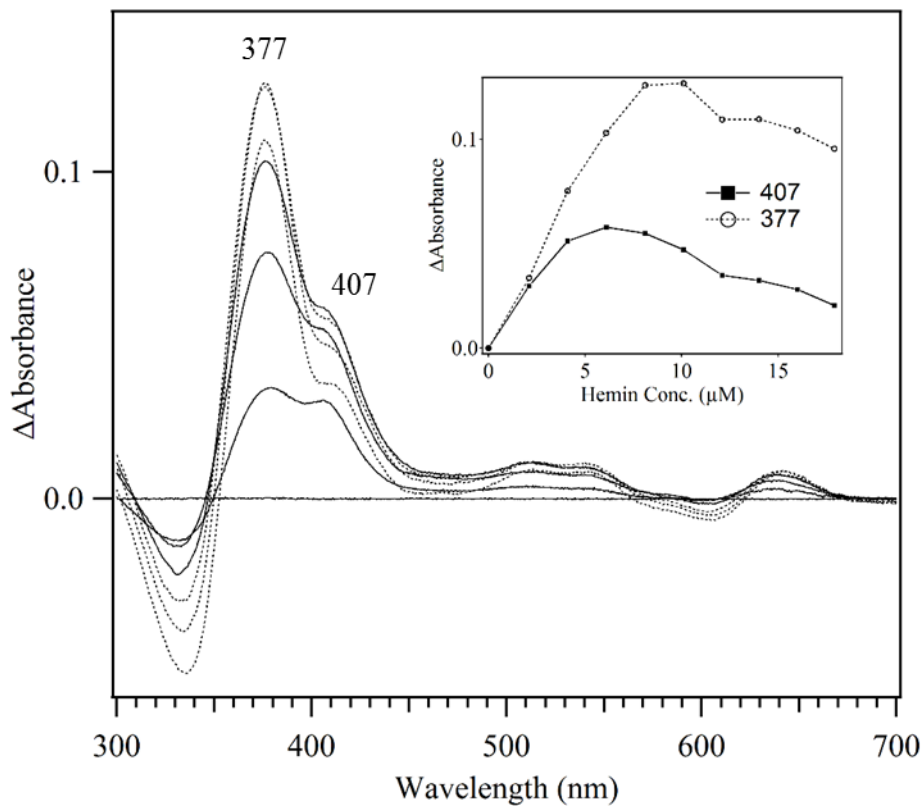


C**Y239F****D****Y239F/R241V**

E R142V



F R241V



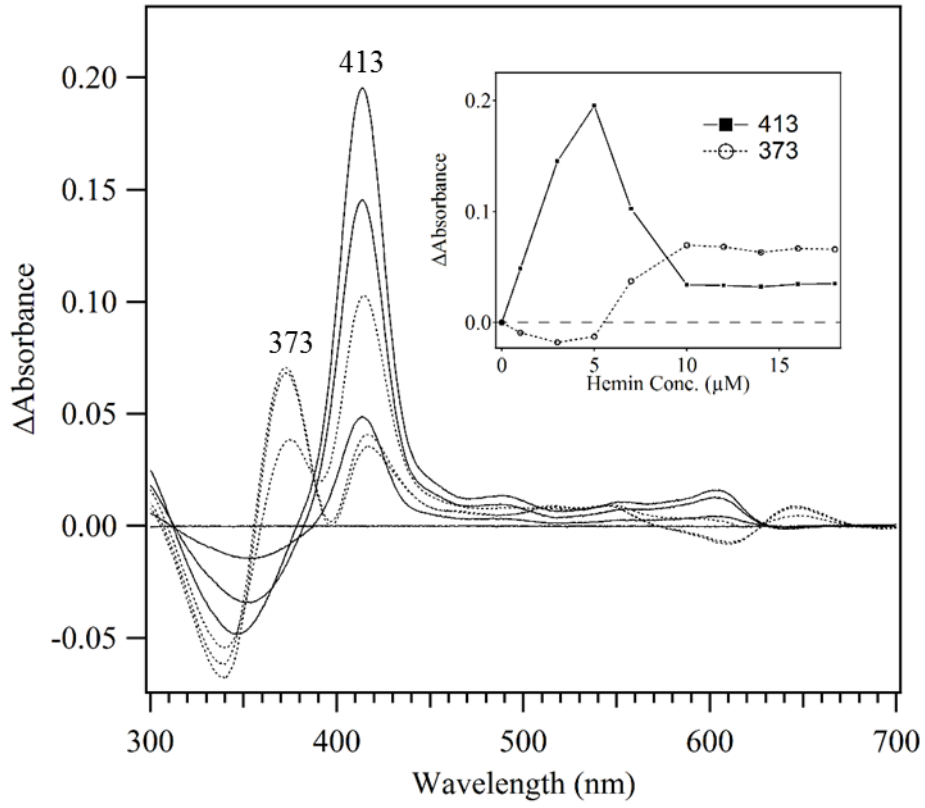
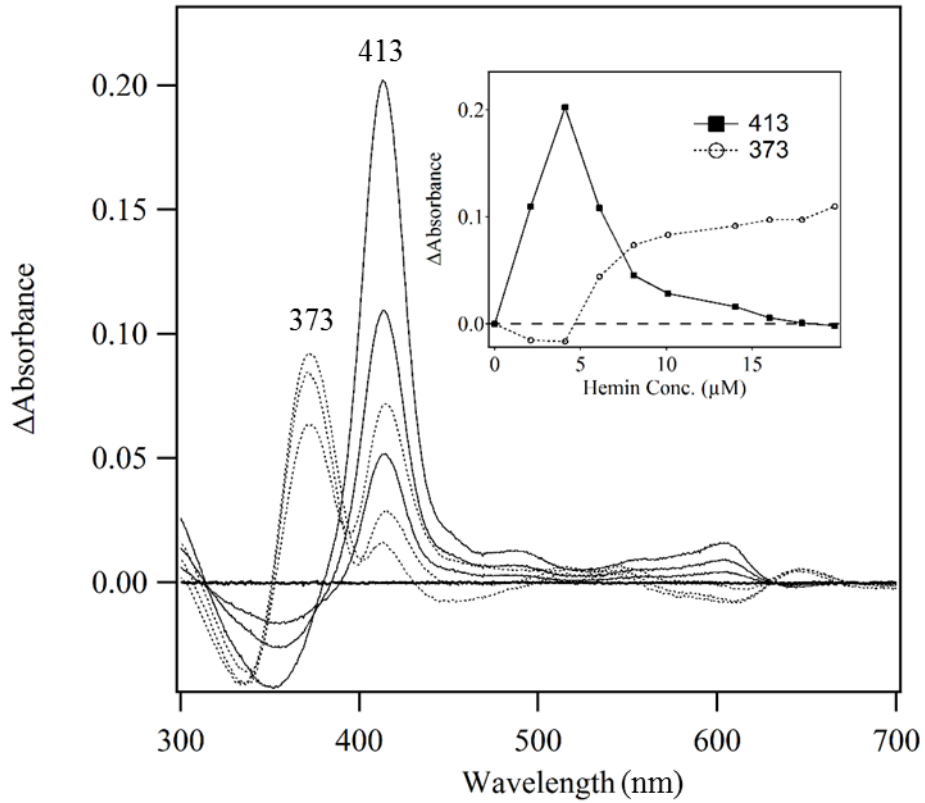
G**F276A****H****L295A**

Figure 18. The UV/vis absorption difference spectra of RhuT mutants in the hemin titration. The UV-visible difference spectra of the hemin titration of RhuT mutants (A) Y140F, (B) Y140F/R142V, (C) Y239F, (D) Y239F/R241V, (E) R142V, (F) R241V, (G) F276A and (H) L295A are plotted. Although the hemin was added in 1 μM steps into a sample cuvette containing 5 μM of purified protein and a reference cuvette containing only buffer (50 mM Tris-HCl pH 8.0), few spectra are presented here for clarity. The change in the value in absorption maxima against hemin concentration is plotted in the inset.

4-8-2 Crystal structure of a mutant in the heme-binding form

Crystals of RhuT mutant Y239F were obtained in the presence of high concentration of hemin (protein: hemin = 1:2) (Figure 19). The crystal structure of the Y239F mutant of RhuT was determined in the 2-heme-bound form at the resolutions of 2.0 \AA (Figure 20). In the structure, two heme molecules are stacked with a Fe-Fe distance of 4.2 \AA and a heme - heme plane distance of 3.3 \AA . In the case of WT, the orientation of heme_C and heme_N are in the same direction (towards the solvent), whereas in the RhuT mutant Y239F, the heme_C orientation is

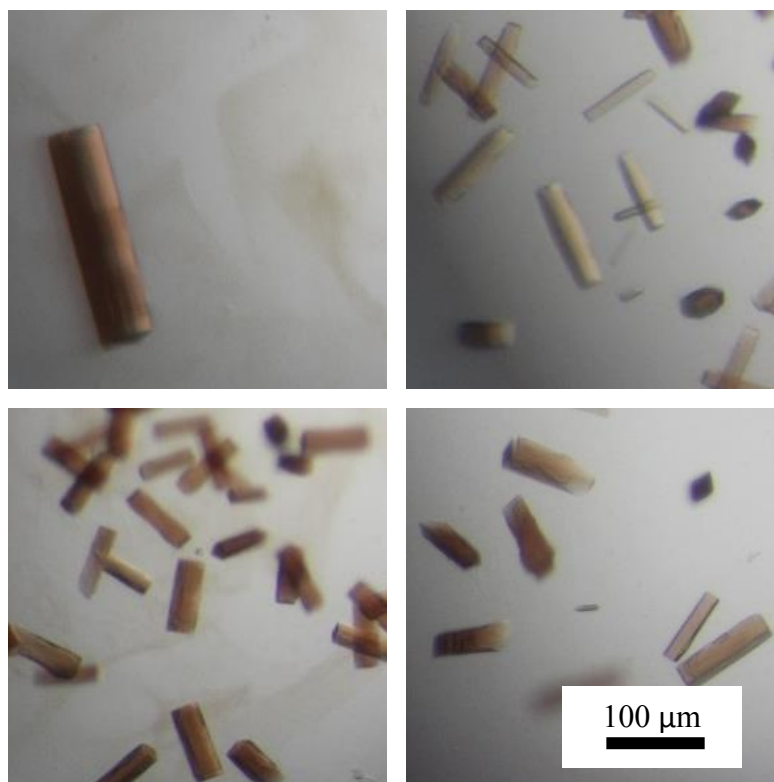


Figure 19. Heme-bound form crystals of RhuT mutant Y239F. The crystals appeared within five days of crystallization by vapor diffusion (sitting drop) method.

opposite compared to the WT (towards inside), while keeping the same orientation of heme_N as WT. The environment of heme_N is the same as that of WT in which Y140 phenolate was coordinated to the heme_N iron as the fifth axial ligand, and interacted with R142 and Q141 via hydrogen bonds. The guanidyl group of R143 also interacted with two propionates of the heme_N. In the case of C-domain side, one water molecule is coordinated with the heme_C and another water molecule is interacting with the propionate of heme_C and A254; and Q247 is interacting with another propionate group of the heme_C.

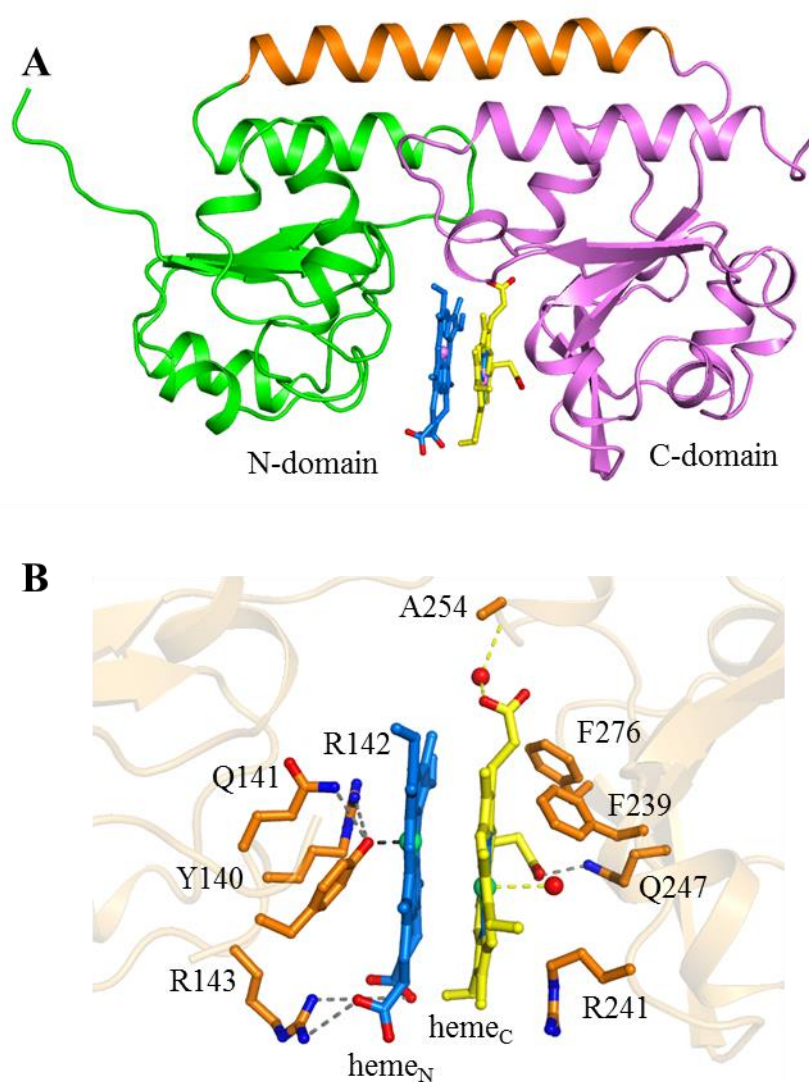


Figure 20. Crystal Structure of RhuT mutant Y239F in 2-heme-binding form. (A) The overall structure of the RhuT mutant Y239F in the 2-heme-bound form, (B) heme-binding cleft of RhuT mutant Y239F showing the heme bound to N-domain as heme_N and heme bound to C-domain as heme_C. Residues in the cleft are showing as stick (orange) and water molecules as sphere (red).

4-8-3 Heme coordination structure of mutants

The resonance Raman (RR) spectra of Tyr mutants of RhuT (Y140F and Y239F) were measured to confirm the coordination structure of the RhuT mutant (Y239F) in the 2-heme-bound form, which was observed by X-ray crystallographic analysis and to understand the difference between WT and mutants. The UV-visible spectra, in the case of WT (Figure 9), in lower hemin concentrations ($<$ protein concentration) only the 1-heme-bound form appeared and then the 2-heme-bound form appeared in higher hemin concentrations ($>$ protein concentration), whereas both mutants (Y140F and Y239F) showed a mixture of the 1-heme- and 2-heme-bound forms even at lower hemin concentrations (Figure 18 A and C). The peak positions were also shifted for mutants compared to WT, indicating the difference in the heme environment among WT and mutants.

In the RR spectra of mutants Y140F and Y239F (Figure 21), like the WT, the ν_4 band which is a characteristic of porphyrin π^* electron density and iron oxidation state, was observed near 1370 cm^{-1} in both lower and high concentration of the hemin into protein, and is indicative of ferric heme. The ν_3 band is the marker band for the heme coordination and the spin-state of heme. In both lower and higher hemin concentration to both RhuT mutants (Y140F and Y239F), the ν_3 band appeared at a range of $1487\text{-}1489\text{ cm}^{-1}$ (Figure 21), indicating the presence of five-coordinate high-spin (5cHS) heme, which was observed in the crystal structure of Y239F mutant. Between the two mutants (Y140F and Y239F), one significant difference is that in lower hemin concentration, a small shoulder peak appeared at 1476 cm^{-1} for the Y140F mutant, showing a mixture of 6cHS and 5cHS hemes.

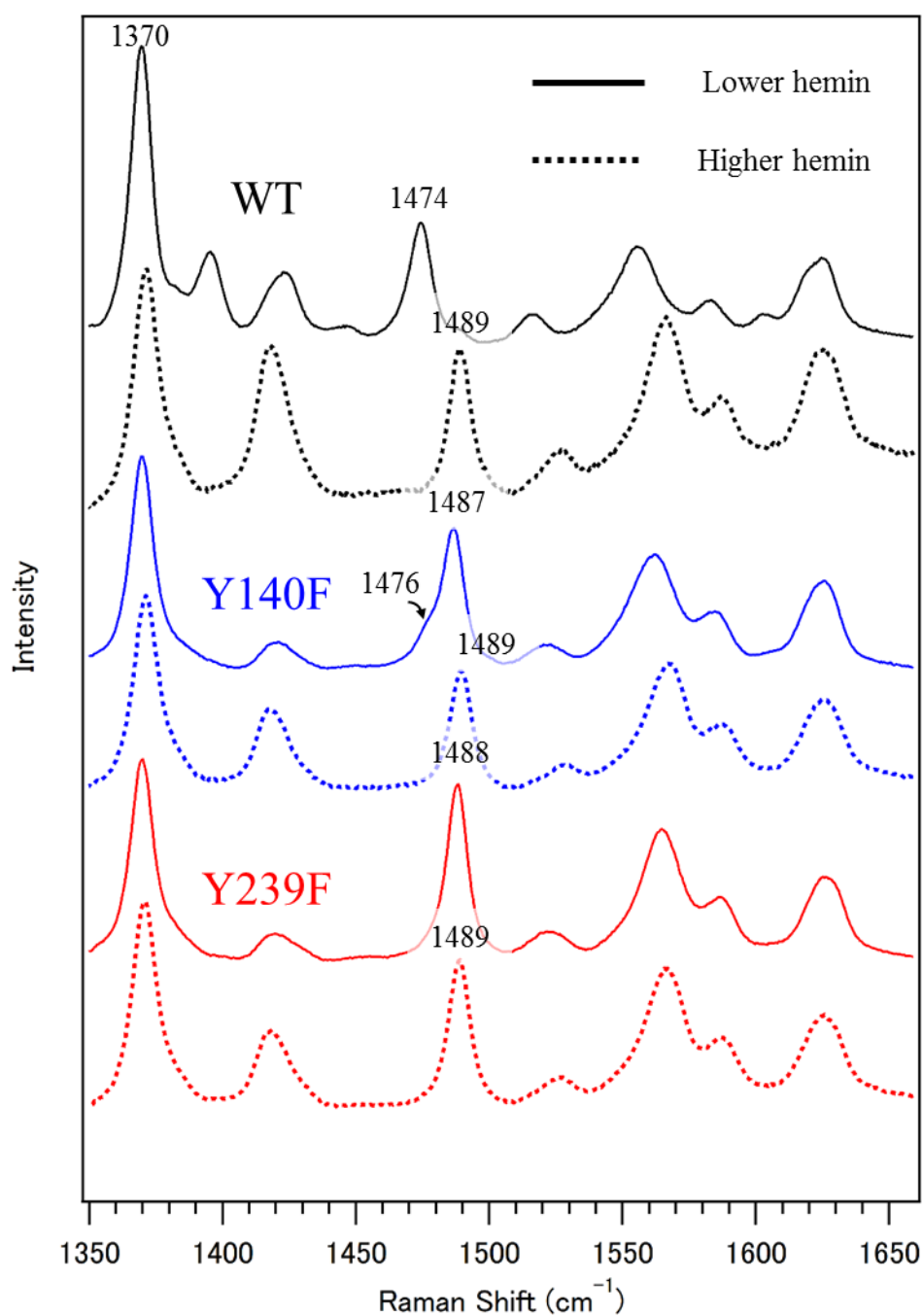


Figure 21. Resonance Raman (RR) spectra of RhuT WT and mutants with addition of hemin. The high-frequency region of resonance Raman spectra of RhuT WT and mutants (WT – black, mutant Y140F - blue, Y239F - red) after adding the hemin solution. The spectra of 25 μM protein with the lower hemin concentration (20 μM) are showing as solid line and the spectra of 25 μM protein with the higher concentration of hemin (52 μM) are showing as dotted line; line with the respective color of WT, mutant Y140F and Y239F. The DMSO was used to dissolve the hemin and showed the bands in the 1418-1423 cm⁻¹ region.

5. DISCUSSION

5-1 Heme-binding mechanism of RhuT

Based on the spectroscopic and crystallographic study of RhuT WT and its mutants, I propose a non-uniform heme-binding model of RhuT as illustrated in Figure 22. The two Tyr from the N-domain and C-domain might have the same level of affinity for heme and the first heme can bind to a Tyr from either domain (Figure 22 A). Then the second heme will bind to the vacant domain. This unique feature of RhuT in the heme-recognition would be a result of two Tyr and the conformational flexibility in the cleft of RhuT by the loop regions. ITC experiment also supports that heme-binding to RhuT do not follow simple sequential binding model (Figure 10). The non-homogeneity in conformation appears to prevent the crystallization of 1-heme-bound form.

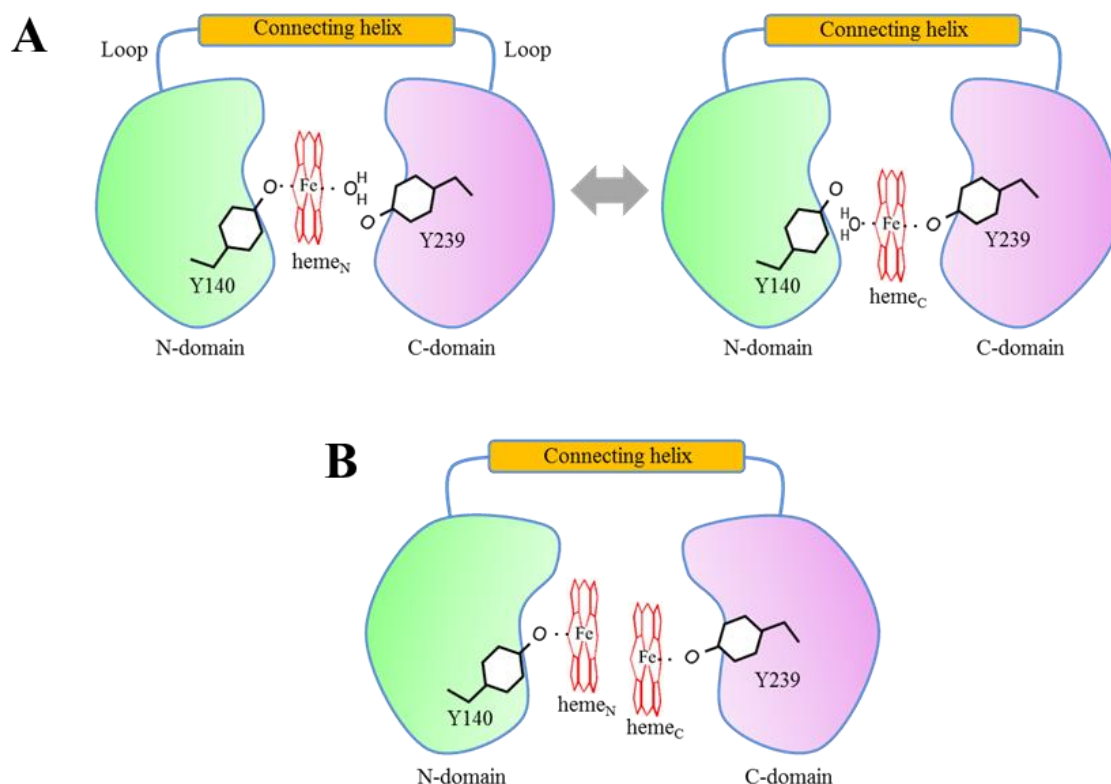


Figure 22. Non-uniform heme-binding mechanism of RhuT. (A) An equilibrium between the 1-heme-bound to either in the N-domain or C-domain, and (B) the 2-heme-bound form.

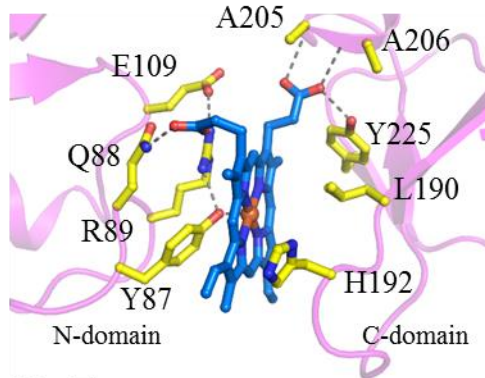
5-2 Similarity and diversity of heme recognition in PBPs

The amino acid sequence of RhuT is homologous to those of 4 other PBPs (~ 36% identity) (Figure 7). However, the orientation of the heme, the heme-binding ligands and the environment of the heme-binding cleft of RhuT were entirely distinct from those of other 4 PBPs, showing diverse recognition of the heme by PBPs. The spectroscopic and thermodynamic analysis also demonstrated the diverse modes of heme recognition.

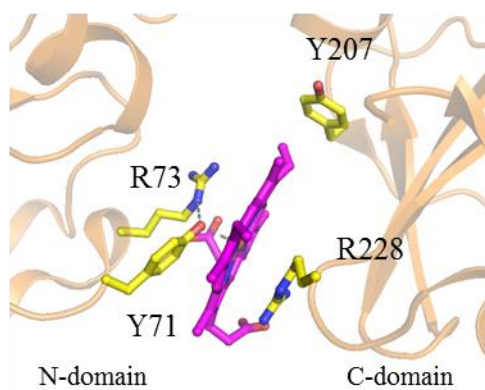
The present study enables to compare the crystal structures of RhuT with the reported structures of homologues BhuT, HmuT, PhuT, and ShuT (Figure 23). The comparison provided a structural basis for the recognition of the heme in PBP and of the conformational changes upon heme binding. Of the PBP-heme interaction, the most conserved feature is the Tyr phenolate coordination to the heme iron as a fifth ligand. The significance of the Tyr binding to the heme in the heme acquisition system has been comprehensively discussed on the basis of crystallographic, UV-vis, magnetic circular dichroism (MCD), and resonance Raman spectroscopic data.^{11, 22} In addition, the cationic residues (Arg or Lys) interacting with the Tyr ligand in the N-domain are also conserved in primary and tertiary structures of PBPs (Figure 22). The significance of the Tyr-Arg interaction in heme-binding proteins has been examined extensively.¹⁰ This interaction has been observed not only in PBPs but also in catalase,²³ as a common structural motif in tyrosinate-coordinated heme proteins. Therefore, it is highly plausible that the Tyr-Arg would stabilize the deprotonated state of Tyr (phenolate) and the Fe³⁺-Tyr bonds, thereby resulting in heme binding with high affinity. Indeed, isothermal titration calorimetry (ITC) experiments of BhuT and HmuT have shown that heme exhibits a high affinity.^{11, 13} In addition, the extracellular heme acquisition protein HasA from *Serratia marcescens*²⁴ uses Tyr as a heme ligand. Unlike PBP, HasA uses His to stabilize the coordination of Tyr to the iron. The elimination of the Tyr-His interaction of HasA by the substitution of His is reported to lower the affinity to heme by 2 orders of magnitude.²⁵ The NEAT domains of cell-wall-anchored Isd proteins from *Staphylococcus aureus*²⁶⁻²⁹ also use Tyr as a ligand for the heme. In NEAT, another Tyr interacts with Tyr ligand. Thus, the structural characteristics of a conserved heme ligand is essential for the tight heme binding in PBP, because PBP have to maintain the high affinity in the periplasm to protect the cell from high cyto-toxicity of the free heme.³⁰

(A) 1-heme bound

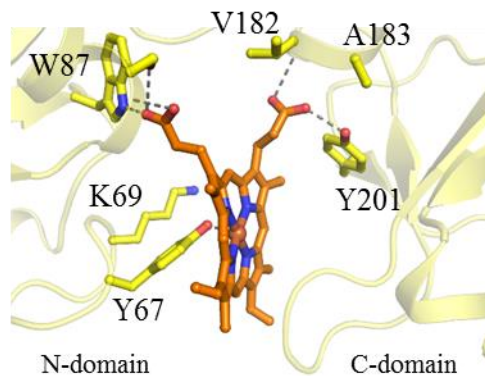
BhuT



PhuT

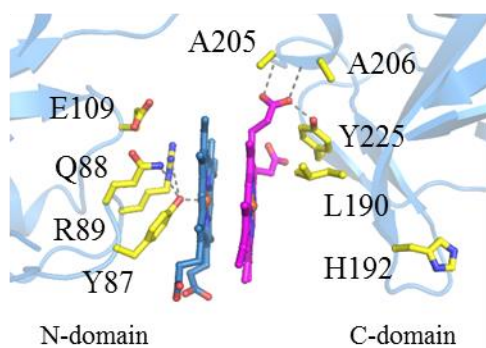


ShuT

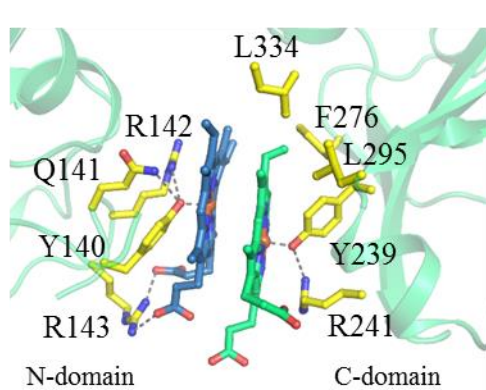


(B) 2-heme bound

BhuT



RhuT



HmuT

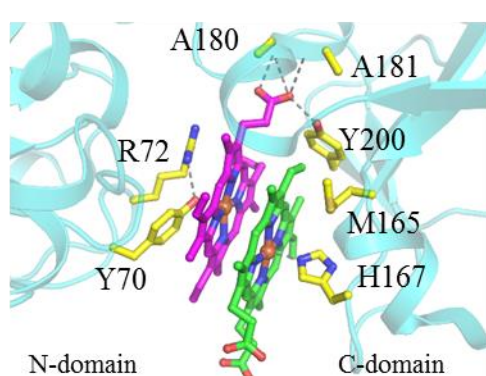


Figure 23. Comparison of the heme-binding cleft among the PBPs from different species. Crystal structures of (A) the 1-heme-bound or (B) 2-heme-bound forms are shown for BhuT (PDB code: 5Y89, 5Y8A), RhuT (PDB Code: 5GJ3), HmuT (PDB code: 3NU1), PhuT (PDB code: 2R79), and ShuT (PDB code: 2R7A). All the PBPs exhibit the same fold in their overall structure. However, the orientation of the heme(s) and most of the residues for heme recognition in the cleft differ among species with the exception of the Tyr-Arg (or Lys) pair of the N-domain.

On the other hand, other features observed in the interactions of the heme with PBP are the diverse recognitions including the numbers of acceptable heme molecules, the heme orientation, and interacting residues of the C-terminal domain in the cleft. The structures of the 1-heme-bound form have been characterized as ShuT, PhuT, and BhuT, while those of the 2-heme-bound form include RhuT, BhuT and HmuT (Figure 23). In the 1-heme-bound form, the heme propionates in BhuT and ShuT are buried, while that in PhuT points toward solvent. In the 2-heme-bound form, the heme_N and heme_C exhibit different orientations in BhuT, but their orientations of HmuT are reverse of BhuT. In RhuT, propionates of both of two hemes point outward to the solvent.

One example of the diversity in heme-protein interaction includes another conserved Tyr (except RhuT, in the case of RhuT: F276) in the C-terminal domain (Figure 22), which interacts with the heme in a variety of manners. The Y201 in ShuT or the Y225 in the 1-heme-bound form of BhuT interacts with one of the heme propionates, while there is no such hydrogen-bonding interaction in the Y207 of PhuT (Figure 23), due to an exposure of the heme propionates to the solvent. In the 2-heme-bound form, the Y200 in HmuT interacts with one propionate of heme_N, while the Y225 in BhuT interacts with one propionate of heme_C. Such diversities in recognition of the heme by the residues of the C-terminal domain likely provide a tolerance for the different orientation of the heme in the cleft of PBP. These structural comparisons suggest the possible mechanism of the heme transfer to TMD: the heme orientation in the PBP cleft might have no significant relevance to the mechanism of transferring the heme from a PBP to a TMD of ABC heme importer.

However, there is no direct evidence that suggests the binding of a stacked pair of hemes is physiologically relevant. In addition, orientations of the heme in PBP might be affected by the mechanism of the heme transfer from TonB-dependent heme receptor in the outer membrane to PBP. Therefore, the present structural data do not exclude the possibility that there are system-dependent mechanistic preferences for particular heme orientations in the PBPs. With respect to the 1- or 2-heme(s) binding to PBP, Locher and co-workers have discussed the possible biological significance in the function of ABC heme importers,¹¹ on the basis of the crystal structure of the 2-heme-bound form of HmuT, and implied that the import of 2-heme molecules in one reaction cycle of the ABC heme importer could be energetically feasible, since most ABC transporters are thought to hydrolyze two ATP molecules during one reaction

cycle. In addition, since HmuT has Tyr and His ligands for the heme from the N- and C-domains, respectively, they also suggested¹¹ that the presence of His in a corresponding position in C-domain in the primary structure (Figure 24) can predict a 2-heme-binding. Although the His residue (H192) in the C-domain is present in a corresponding position of BhuT, it does not bind to the iron in the 1-heme-bound form of BhuT, and swings out from the heme-binding cleft in the 2-heme-bound form, as were observed in the crystal structures and resonance Raman spectra¹³. Therefore, it was suggested that the Fe-His coordination is not necessarily required for the heme binding in BhuT. In the case of RhuT, there are two Tyr-Arg motifs in the cleft, i.e., Y140-R142 in the N-domain and Y239-R241 in the C-domain. The site-directed mutagenesis experiments showed that all of the single and double mutants of these four residues of RhuT retained the 2-heme binding ability (Figure 18). Based on these results, I suggest that the second ligand residue in the heme cleft are not highly responsible for the determination of one- or 2-heme(s) binding. Rather, conformational flexibility with the residues of the heme cleft are the structural factors controlling 1- or 2-heme binding in PBPs.

5-3 Evolution of bacteria and PBPs

Figure 24 illustrates the sequence alignment of some PBPs from thermophile and proteobacteria and some heme-binding proteins from Gram-positive bacteria. The thermophile is showing the existence of the two Tyr as heme ligands symmetrically located on both N-domain and C-domain regions (RhuT). For all orthologues, one Tyr from either domain seems much conserved, indicating an essential role of Tyr for heme-binding. It is interesting that the sequence alignment show that some proteiobacteria have a His residue (marked by blue color) in the same place of the C-domain and two of them reported to bind two hemes (BhuT, HmuT). On the other hand, ShuT and PhuT do not have a His in that position of the C-domain and reported to bind with only one heme. I propose that the common ancestor of PBPs might have two domains with Tyr in each domain, but one Tyr survived to maintain the affinity of the heme. On the other hand, the residues in the cleft except one Tyr ligand might evolve divergently to less specific interaction to facilitate the heme dissociation.

	N-domain										C-domain														
	140										239														
<i>Roseiflexus</i> Sp. (RhuT)	P	N	I	_	G	Y	Q	R	R	L	S	A	E	V	L	F	L	Y	L	R	G	T	D	Thermophile
<i>T. thermophilus</i>	P	S	V	_	G	Y	Q	F	R	L	S	A	E	A	L	F	L	Y	L	R	G	P	G	
<i>D. geothermalis</i>	P	K	V	_	G	Y	Q	R	S	L	S	A	E	V	M	F	I	Y	A	R	G	P	Q	
<i>B. cenocepacia</i> (BhuT)	P	K	V	_	G	Y	Q	R	A	L	S	A	E	V	L	F	V	L	N	H	T	G	T	Proteobacteria
<i>K. pneumoniae</i>	P	D	V	_	G	Y	L	R	Q	L	N	A	E	V	L	F	I	L	S	H	G	G	M	
<i>Y. pestis</i> (HmuT)	P	D	V	_	G	Y	M	R	T	L	N	A	E	V	L	F	V	M	S	H	G	G	L	
<i>A. fischeri</i>	P	K	I	_	G	Y	H	R	Q	L	S	T	E	V	I	Y	L	L	L	H	E	G	R	
<i>P. aeruginosa</i> (PhuT)	P	S	V	_	G	Y	Q	R	Q	L	A	A	E	V	L	L	V	I	G	N	A	G	G	
<i>S. dysenteriae</i> (ShuT)	P	H	I	_	G	Y	W	K	Q	L	S	S	E	A	M	F	I	L	S	A	G	G	S	
<i>R. opacus</i>	P	V	V	T	P	G	G	Q	S	L	N	A	E	I	A	F	L	Y	L	R	G	T	A	Gram-positive
<i>C. acnes</i>	P	V	V	T	E	N	G	H	V	L	N	V	E	V	A	F	L	Y	V	R	G	N	A	
<i>C. diphtheriae</i>	P	V	V	T	E	G	G	H	N	I	N	V	E	V	A	F	L	Y	A	R	G	N	G	

Figure 24. Sequence alignment of some orthologues of RhuT. The alignment is showing the region of heme ligand residues in the N-domain and C-domain. The heme liganded Tyr residues are marked by red color. The background of thermophile are colored by yellow, the proteobacteria with a conserved His in C-domain colored by light-green (His marked by blue color) and the proteobacteria without His are colored by green. Gram positive bacteria colored by cyan.

5-4 Conformational changes in PBPs during heme transfer to the transporter

In the present study, the “open” and “closed” conformation of PBPs can be defined in terms of the distance between the $C\alpha$ atoms of two well-conserved Glu residues (Figure 25). In the comparison of multiple states of conformation for three PBPs, the apo and 2-heme-bound forms show open conformation and the 1-heme-bound form shows a closed conformation. Since these two Glu residues are interaction sites with the TMD, the “open” or “closed” conformation of PBP when it associates with TMD during heme transport could be discussed.

The structure of a full complex of an ABC heme importer BhuUV-T from *B. cenocepacia* has been reported³¹ (PDB code: 5B58) in heme and nucleotide free state, where BhuT is in the apo form and dimerized BhuU (TMD) is in an inward-facing conformation, wherein the pathway

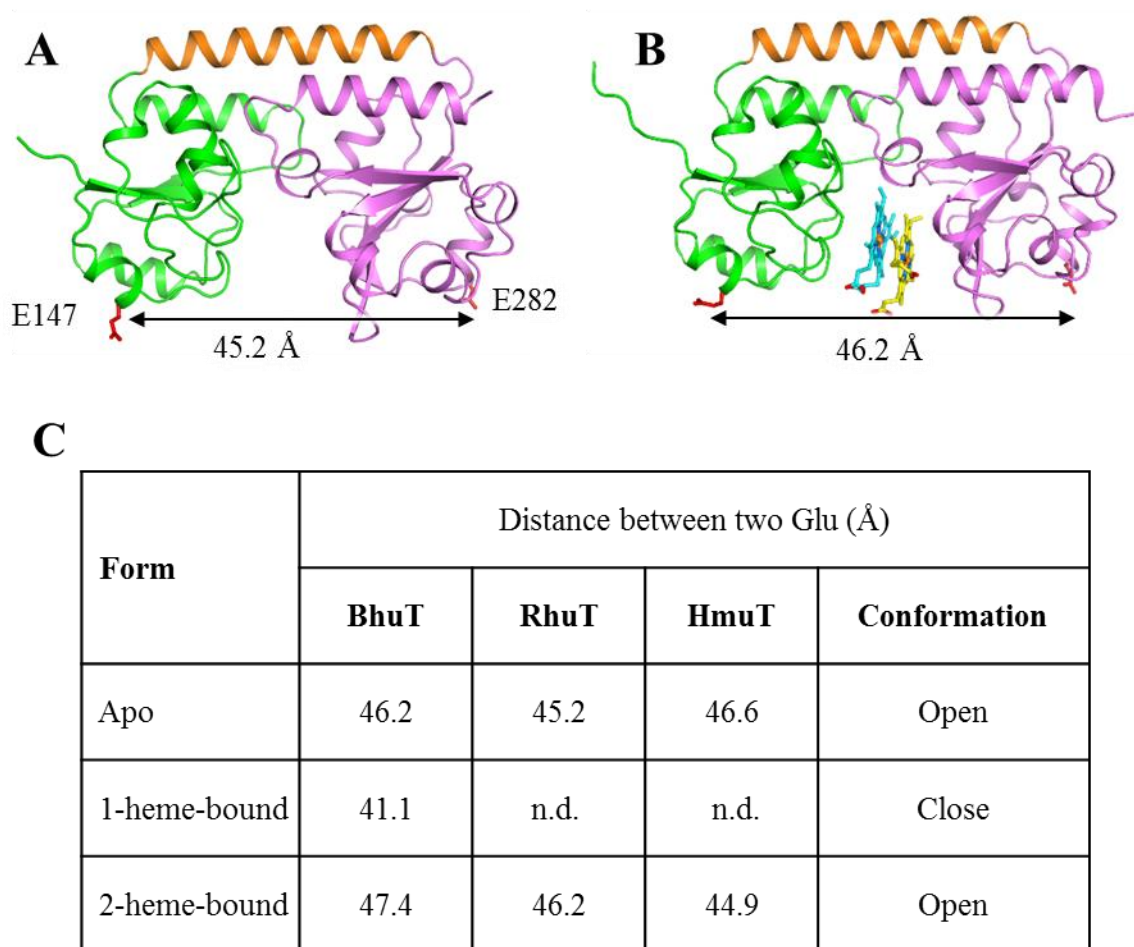


Figure 25. Conformational changes in PBPs during heme-binding. Crystal structures of RhuT in (A) apo and (B) 2-heme-bound forms. (C) Table shows the distance between two conserved Glu on the surface in different states of conformation of PBPs. (n.d.: no data available)

for heme import is opened toward the cytoplasmic side and closed at the periplasmic gate (Figure 26A). BhuT interacts with the periplasmic surface of BhuU through the electrostatic interaction of the two conserved Glu residues of BhuT (E94 and E231) with the two Arg residues (R84) of each subunit of a dimerized BhuU. The distance between the two Glu residues of BhuT in the BhuUV-T complex was 47.5 Å, and the distance between the Arg84 and Arg84 of BhuU dimer was 49.5 Å. The Glu-Glu distance of BhuT in the complex was comparable to those of apo (46.2 Å) and 2-heme-bound form (47.4 Å) of BhuT, suggesting that the BhuT in the BhuUV-T complex should be in an “open” conformation. Unfortunately, a structure of PBP-TMD complex where TMD in the outward facing conformation is not yet available. On the other hand, the structure of another ABC-heme importer, HmuUV in the TMD-NBD complex from *Y. pestis* was reported³² in heme and nucleotide free state. Although its cognate PBP

(HmuT) was not bound, the HmuU (TMD) in the HmuUV complex was in the outward facing conformation, in which the periplasmic gate of the heme translocation channel was open (Figure 26B).

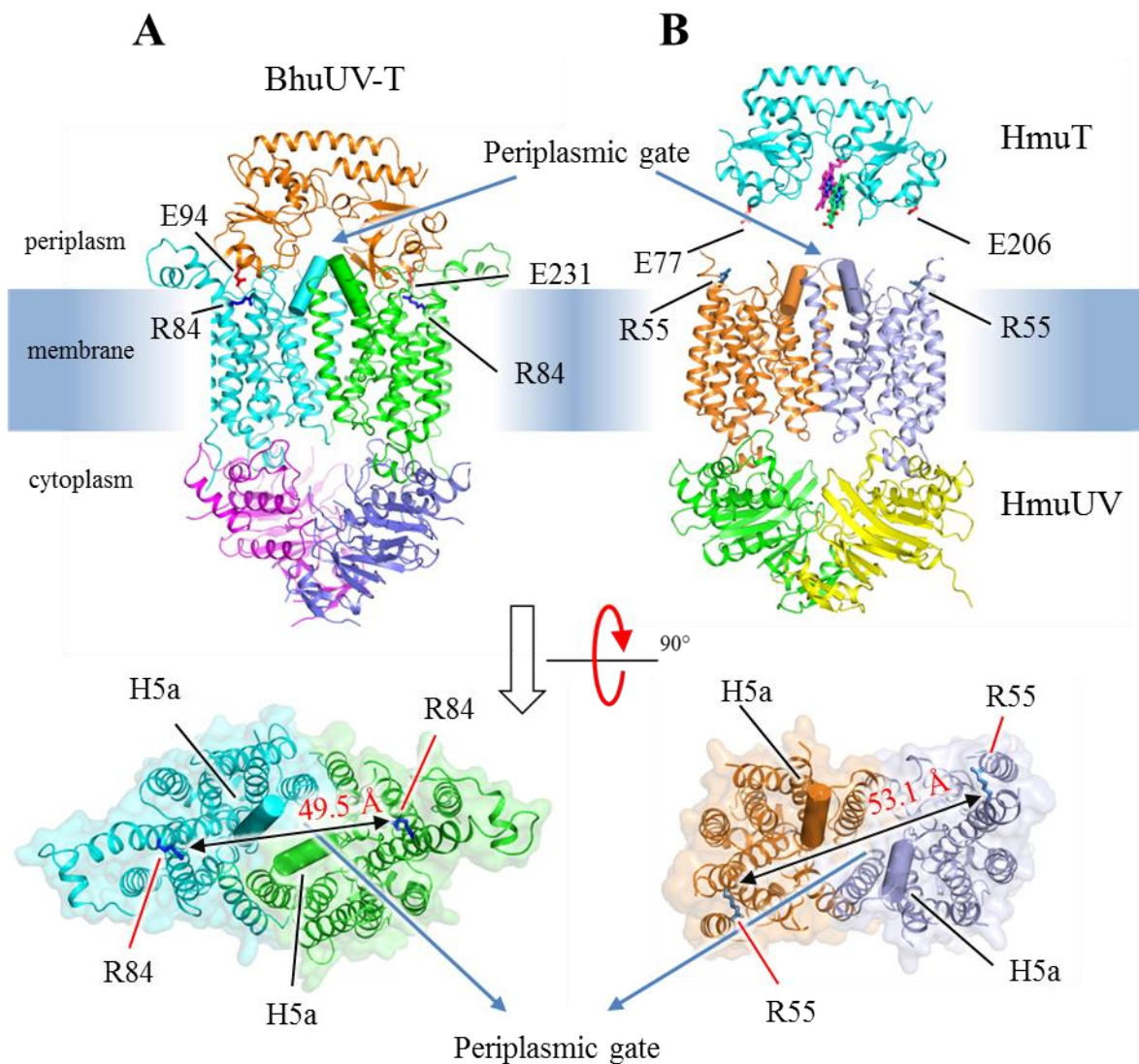


Figure 26. The crystal structures of the heme importer. (A) *Burkholderia cenocepacia* BhuUV-T complex (PDB code: 5B58) and (B) *Yersinia pestis* HmuUV (PDB code: 4G1U); HmuT (PDB code: 3NU1). Two conserved glutamate residues of PBP (E94 and E231 of BhuT, and E77 and E206 of HmuT) and two conserved arginine residues of TMD (R84 of BhuU and R55 of HmuU) are shown as stick models. The periplasmic gate is situated between two H5a helices that are shown as a cylinder. In the BhuUV-T complex, the periplasmic gate is completely closed while it is open in HmuUV structure. The distances between two conserved arginine residues in TMD are 49.5 and 53.1 Å for BhuUV and HmuUV, respectively.

Since all transporter from these orthologues exhibits higher similarity in the amino acid sequences, similarities in the tertiary structures seem likely. In this HmuUV complex, the distance between the two R55 residues in the TMD dimer was 53.1 Å. When the heme-bound PBP forms a complex with TMD in the outward-facing conformation, the conserved Glu-Glu distance in the PBP should be around 51 Å in order to maintain the Glu-Arg interaction like the interaction was observed in the BhuUV-T complex. The Glu-Glu distance in the complex should be longer than that of 2-heme-bound form of HmuT (44.9 Å) in the “open conformation,” and was much longer than that of the 1-heme-bound form of BhuT (41.1 Å) in the “closed conformation.”

Therefore, I suggest that a complex formation of heme(s)-bound PBPs with a heme transporter in the outward facing conformation would transform the PBPs into a “more open” conformation (Figure 27), in which the heme-binding cleft of the PBP must be opened more than that of even the isolated 2-heme-bound form. This conformational change in the heme cleft of PBP could weaken or disrupt interactions of the heme(s) with its (their) surroundings, including the heme-Tyr coordination bond. Such conformational change might be a trigger to the heme transfer from the hydrophilic cleft of PBP to the hydrophobic channel of TMD.

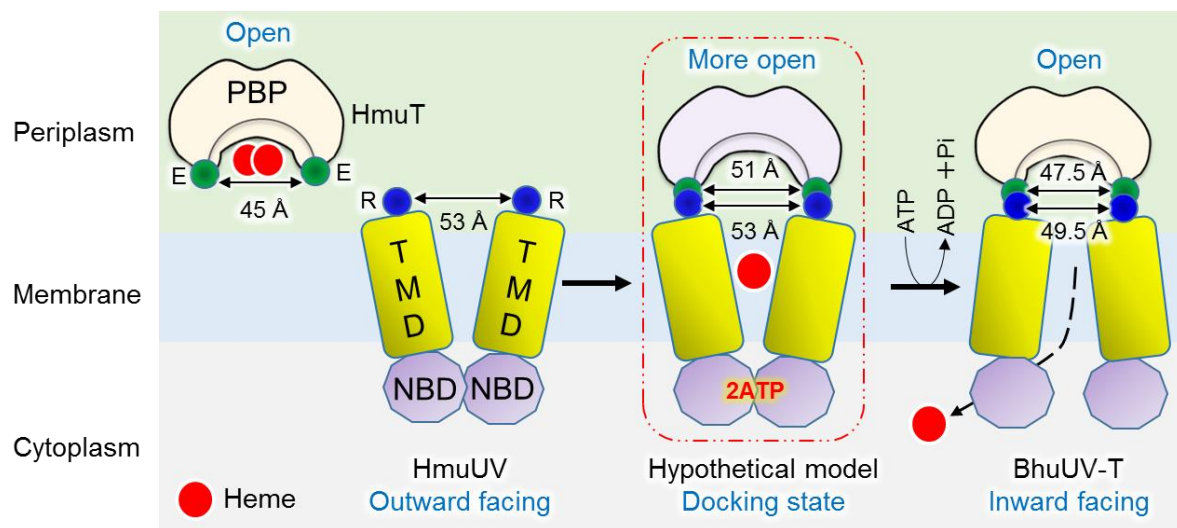


Figure 27. The alternative access mechanism of ABC transporter. After heme-binding, heme-bound PBP will dock with the outward facing conformation of TMD (hypothetical model) and PBP will release the heme to the TMD of the transporter. Upon ATP-hydrolysis, the TMD will change to inward facing conformation (BhuUV-T), which enable the heme entry to cytoplasm.

6. CONCLUSION

PBPs in the bacterial heme-acquisition systems can capture heme molecules in a heme-binding cleft, via Tyr coordination to the heme iron, but various interactions with cleft residues accompany an “open” or “closed” conformational change. The conserved Tyr-Arg linkage observed in the heme iron ligand of PBPs possibly stabilizes the deprotonated state of Tyr and would function as an effective heme-capturing system. The heme cleft of PBPs can adopt “closed,” “open” or “more open” conformations, depending on the heme concentration and on binding to the cognate TMD of the heme importer. Since PBPs themselves possess an effective heme capturing system, as described above, it is unlikely that the heme dissociates from PBPs without any conformational changes. Namely, the “more open” conformation of a PBP upon binding to a TMD would be responsible for the heme transfer. Therefore, for the heme-acquisition systems of Gram-negative bacteria, I propose that the conformational changes within the domain motion of PBPs control the affinity of the heme, and could be important for the heme transport from PBP to the TMD.

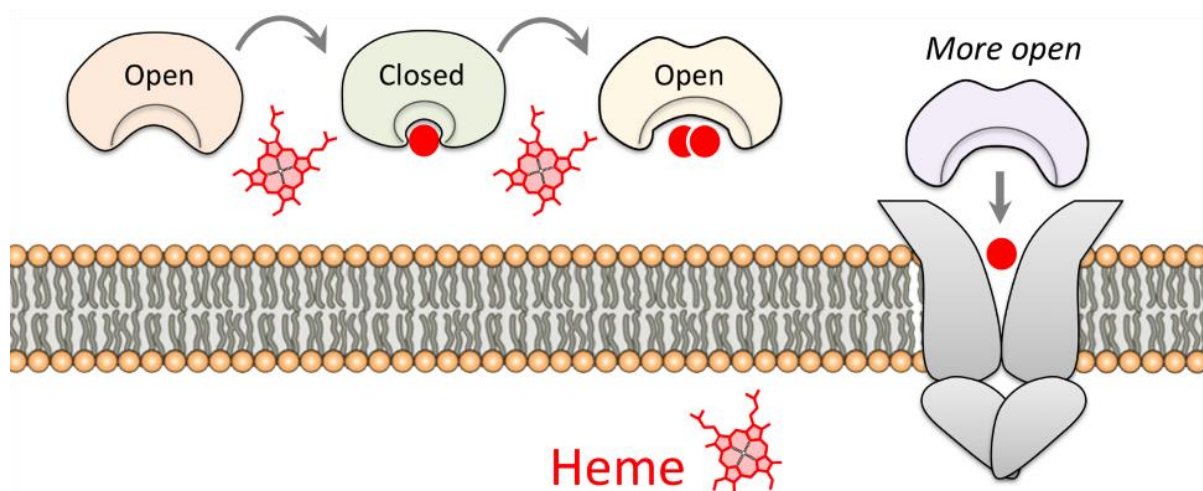


Figure 28. Model of heme-binding and release from PBP. PBPs can bind 1 or 2 heme molecules depending on the heme concentration. The cleft of PBPs can adopt closed and open conformation during binding with heme(s), and a more open conformation during docking with dimeric TMD.

7. REFERENCES

- (1) Ilbert, M., and Bonnefoy, V. (2013) Insight into the evolution of the iron oxidation pathways, *Biochim. Biophys. Acta* 1827, 161-175.
- (2) Braun, V., and Hantke, K. (2011) Recent insights into iron import by bacteria, *Curr. Opin. Chem. Biol.* 15, 328-334.
- (3) Noinaj, N., Guillier, M., Barnard, T. J., and Buchanan, S. K. (2010) TonB-dependent transporters: regulation, structure, and function, *Annu. Rev. Microbiol.* 64, 43-60.
- (4) Contreras, H., Chim, N., Credali, A., and Goulding, C. W. (2014) Heme uptake in bacterial pathogens, *Curr. Opin. Chem. Biol.* 19, 34-41.
- (5) Rees, D. C., Johnson, E., and Lewinson, O. (2009) ABC transporters: the power to change, *Nat. Rev. Mol. Cell. Biol.* 10, 218-227.
- (6) O'Neill, M. J., and Wilks, A. (2013) The *P. aeruginosa* heme binding protein PhuS is a heme oxygenase titratable regulator of heme uptake, *ACS Chem. Biol.* 8, 1794-1802.
- (7) Mayfield, J. A., Dehner, C. A., and DuBois, J. L. (2011) Recent advances in bacterial heme protein biochemistry, *Curr. Opin. Chem. Biol.* 15, 260-266.
- (8) Quioco, F. A., and Ledvina, P. S. (1996) Atomic structure and specificity of bacterial periplasmic receptors for active transport and chemotaxis: variation of common themes, *Mol. Microbiol.* 20, 17-25.
- (9) Berntsson, R. P., Smits, S. H., Schmitt, L., Slotboom, D. J., and Poolman, B. (2010) A structural classification of substrate-binding proteins, *FEBS Lett.* 584, 2606-2617.
- (10) Ho, W. W., Li, H., Eakanukul, S., Tong, Y., Wilks, A., Guo, M., and Poulos, T. L. (2007) Holo- and apo-bound structures of bacterial periplasmic heme-binding proteins, *J. Biol. Chem.* 282, 35796-35802.
- (11) Mattle, D., Zeltina, A., Woo, J. S., Goetz, B. A., and Locher, K. P. (2010) Two stacked heme molecules in the binding pocket of the periplasmic heme-binding protein HmuT from *Yersinia pestis*, *J. Mol. Biol.* 404, 220-231.
- (12) Patzlaff, J. S., van der Heide, T., and Poolman, B. (2003) The ATP/substrate stoichiometry of the ATP-binding cassette (ABC) transporter OpuA, *J. Biol. Chem.* 278, 29546-29551.

- (13) Naoe, Y., Nakamura, N., Rahman, M. M., Tosha, T., Nagatoishi, S., Tsumoto, K., Shiro, Y., and Sugimoto, H. (2017) Structural basis for binding and transfer of heme in bacterial heme-acquisition systems, *Proteins* 85, 2217-2230.
- (14) Berry, E. A., and Trumpower, B. L. (1987) Simultaneous determination of hemes a, b, and c from pyridine hemochrome spectra, *Anal. Biochem.* 161, 1-15.
- (15) Collaborative Computational Project, N. (1994) The CCP4 suite: programs for protein crystallography, *Acta Crystallogr., Sect. D: Biol. Crystallogr.* 50, 760-763.
- (16) McCoy, A. J., Grosse-Kunstleve, R. W., Adams, P. D., Winn, M. D., Storoni, L. C., and Read, R. J. (2007) Phaser crystallographic software, *J. Appl. Crystallogr.* 40, 658-674.
- (17) Cowtan, K. (1994) DM: an automated procedure for phase improvement by density modification., *Joint CCP4 and ESF-EACBM Newsletter on Protein Crystallography* 31, 34-38.
- (18) Langer, G., Cohen, S. X., Lamzin, V. S., and Perrakis, A. (2008) Automated macromolecular model building for X-ray crystallography using ARP/wARP version 7, *Nat. Protoc.* 3, 1171-1179.
- (19) Emsley, P., Lohkamp, B., Scott, W. G., and Cowtan, K. (2010) Features and development of Coot, *Acta Crystallogr., Sect. D: Biol. Crystallogr.* 66, 486-501.
- (20) Murshudov, G. N., Vagin, A. A., and Dodson, E. J. (1997) Refinement of macromolecular structures by the maximum-likelihood method, *Acta Crystallogr., Sect. D: Biol. Crystallogr.* 53, 240-255.
- (21) Kandt, C., and Tieleman, D. P. (2010) Holo-BtuF stabilizes the open conformation of the vitamin B12 ABC transporter BtuCD, *Proteins* 78, 738-753.
- (22) Draganova, E. B., Akbas, N., Adrian, S. A., Lukat-Rodgers, G. S., Collins, D. P., Dawson, J. H., Allen, C. E., Schmitt, M. P., Rodgers, K. R., and Dixon, D. W. (2015) Heme Binding by *Corynebacterium diphtheriae* HmuT: Function and Heme Environment, *Biochemistry* 54, 6598-6609.
- (23) Fita, I., and Rossmann, M. G. (1985) The active center of catalase, *J. Mol. Biol.* 185, 21-37.

- (24) Arnoux, P., Haser, R., Izadi, N., Lecroisey, A., Delepierre, M., Wandersman, C., and Czjzek, M. (1999) The crystal structure of HasA, a hemophore secreted by *Serratia marcescens*, *Nat. Struct. Biol.* 6, 516-520.
- (25) Caillet-Saguy, C., Turano, P., Piccioli, M., Lukat-Rodgers, G. S., Czjzek, M., Guigliarelli, B., Izadi-Pruneyre, N., Rodgers, K. R., Delepierre, M., and Lecroisey, A. (2008) Deciphering the structural role of histidine 83 for heme binding in hemophore HasA, *J. Biol. Chem.* 283, 5960-5970.
- (26) Sharp, K. H., Schneider, S., Cockayne, A., and Paoli, M. (2007) Crystal structure of the heme-IsdC complex, the central conduit of the Isd iron/heme uptake system in *Staphylococcus aureus*, *J. Biol. Chem.* 282, 10625-10631.
- (27) Grigg, J. C., Mao, C. X., and Murphy, M. E. (2011) Iron-coordinating tyrosine is a key determinant of NEAT domain heme transfer, *J. Mol. Biol.* 413, 684-698.
- (28) Grigg, J. C., Vermeiren, C. L., Heinrichs, D. E., and Murphy, M. E. (2007) Haem recognition by a *Staphylococcus aureus* NEAT domain, *Mol. Microbiol.* 63, 139-149.
- (29) Watanabe, M., Tanaka, Y., Suenaga, A., Kuroda, M., Yao, M., Watanabe, N., Arisaka, F., Ohta, T., Tanaka, I., and Tsumoto, K. (2008) Structural basis for multimeric heme complexation through a specific protein-heme interaction: the case of the third neat domain of IsdH from *Staphylococcus aureus*, *J. Biol. Chem.* 283, 28649-28659.
- (30) Anzaldi, L. L., and Skaar, E. P. (2010) Overcoming the heme paradox: heme toxicity and tolerance in bacterial pathogens, *Infect. Immun.* 78, 4977-4989.
- (31) Naoe, Y., Nakamura, N., Doi, A., Sawabe, M., Nakamura, H., Shiro, Y., and Sugimoto, H. (2016) Crystal structure of bacterial haem importer complex in the inward-facing conformation, *Nat. Commun.* 7, 13411.
- (32) Woo, J. S., Zeltina, A., Goetz, B. A., and Locher, K. P. (2012) X-ray structure of the *Yersinia pestis* heme transporter HmuUV, *Nat. Struct. Mol. Biol.* 19, 1310-1315.

8. ACKNOWLEDGEMENTS

Firstly, I would like to express my sincere gratitude to my supervisor Professor **Yoshitsugu Shiro**, you have been a great mentor to me. I would like to thank for your guidance, suggestion, and encouragement during my Ph.D. study and for allowing me to grow as a research scientist. Your advice on both research as well as on my career has been invaluable. Next, I would like to thank my co-supervisor Dr. **Hiroshi Sugimoto**, Senior Research Scientist, RIKEN SPring-8 Center. I feel lucky to have the opportunity to learn structural biology from a great scientist like you, thank you for your patience, encouragement, suggestion and giving me the laborious training for helping me to understand completely new field from the scratch.

I would like to thank my thesis committee members, Professor **Yoshiki Higuchi**, Professor **Toru Yoshihisa** and Professor **Tsunehiro Mizushima** for your time and patience to hear my research. Thank you for all your brilliant comments, suggestion and encouragement. I also would like to thank Professor **Thomas L. Poulos**, University of California, Irvine and Professor **Shigetoshi Aono**, Institute for Molecular Science for your valuable comments and encouragements.

The thesis work has been done with the support of many people and I would like to thank all my group members, including Dr. **Hiro Nakamura**, Dr. **Tamao Hisano**, Dr. **Takehiko Tosha**, Dr. **Minoru Kubo**, Dr. **Kazumasa Muramoto**, Dr. **Hitomi Sawai** and **Nozomi Nakamura**; for your support and advice during my Ph.D. studies. I like to thank Professor **Kouhei Tsumoto** and Dr. **Satoru Nagatoishi**, The University of Tokyo for helping me to conduct ITC experiments in your laboratory. I also like to thank Professor **Takashi Ogura**, University of Hyogo for allowing me to use your Raman equipment. I thank the beamline scientist Dr. **Keitaro Yamashita**, Dr. **Kunio Hirata** and Professor **Masaki Yamamoto** of SPring-8 for your assistance in the data collection.

I would like to thank the **Leading Program in Doctoral Education** of Graduate School of Life Science, University of Hyogo for the outstanding educational curriculum, funding and financial support. I like to express my deep gratitude to the **Picobiology staffs** and my **friends** for helping me not only to the academic but also in my personal life in Japan. I would like to thank all the Japanese people to whom I met in this four and half years, you all are very kind, polite and helpful; I will miss my Japan life surely. Thank you, **Japan!**

A special thanks to my family. Words cannot express how grateful I am to my father **Md. Badrul Islam** and mother **Latifa Islam**, for all the prayers and sacrifices that you have made on my behalf. I would like to thank my father-in-law **Md. Gyas Uddin** and mother-in-law **Selina Akter**, brother-in-law **Mahabub-uz-Zaman** and sister-in-law **Mahfuza Akter**, thank you for your words of encouragement and support. In the end, I would like to express appreciation to my beloved wife **Masuma Parvin**, you have been my strength all through the times, I want to thank you for supporting me always; and my lovely son **Arham Yeamin** for your great smile to refresh me after a long day at work.